The Plant Cell, Vol. 31: 1308–1327, June 2019, www.plantcell.org © 2019 ASPB.

An RNA Chaperone–Like Protein Plays Critical Roles in Chloroplast mRNA Stability and Translation in Arabidopsis and Maize

Jingjing Jiang,[a,b,1] Xin Chai,[a,b,1] Nikolay Manavski,[c,1,2] Rosalind Williams-Carrier,[d] Baoye He,[a] Andreas Brachmann,[e] Daili Ji,[a] Min Ouyang,[a] Yini Liu,[a] Alice Barkan,[d] Jörg Meurer,[c] Lixin Zhang,[a,f] and Wei Chi[a,b,3]

[a] Photosynthesis Research Center, Key Laboratory of Photobiology, Institute of Botany, Chinese Academy of Sciences, Beijing 100093, China
[b] University of Chinese Academy of Sciences, Beijing 100049, China
[c] Biozentrum der Ludwig-Maximilians-Universität, Plant Molecular Biology, 82152 Planegg-Martinsried, Germany
[d] Institute of Molecular Biology, University of Oregon, Eugene, Oregon 97403
[e] Genetics, Faculty of Biology, Ludwig-Maximilians-University Munich, 82152 Planegg-Martinsried, Germany
[f] Key Laboratory of Plant Stress Biology, State Key Laboratory of Cotton Biology, School of Life Sciences, Henan University, Kaifeng 475004, China

ORCID IDs: 0000-0002-9207-0190 (J.J.); 0000-0002-0763-9574 (X.C.); 0000-0003-2740-5991 (N.M.); 0000-0001-7408-9739 (R.W.-C.); 0000-0003-0401-4955 (B.H.); 0000-0001-7980-8173 (A.B.); 0000-0002-1107-7367 (D.J.); 0000-0001-6040-4312 (M.O.); 0000-0003-1924-7858 (Y.L.); 0000-0003-3049-2838 (A.B.); 0000-0003-2973-9514 (J.M.); 0000-0003-2389-7052 (L.Z.); 0000-0001-6487-002X (W.C.)

A key characteristic of chloroplast gene expression is the predominance of posttranscriptional control via numerous nucleus-encoded RNA binding factors. Here, we explored the essential roles of the S1-domain-containing protein *photosynthetic electron transfer B* (*petB*)/ *petD* Stabilizing Factor (BSF) in the stabilization and translation of chloroplast mRNAs. BSF binds to the intergenic region of *petB-petD*, thereby stabilizing 3′ processed *petB* transcripts and stimulating *petD* translation. BSF also binds to the 5′ untranslated region of *petA* and activates its translation. BSF displayed nucleic-acid-melting activity in vitro, and its absence induces structural changes to target RNAs in vivo, suggesting that BSF functions as an RNA chaperone to remodel RNA structure. BSF physically interacts with the pentatricopeptide repeat protein Chloroplast RNA Processing 1 (AtCRP1) and the ribosomal release factor-like protein Peptide chain Release Factor 3 (PrfB3), whose established RNA ligands overlap with those of BSF. In addition, PrfB3 stimulated the RNA binding ability of BSF in vitro. We propose that BSF and PrfB3 cooperatively reduce the formation of secondary RNA structures within target mRNAs and facilitate AtCRP1 binding. The translation activation function of BSF for *petD* is conserved in Arabidopsis (*Arabidopsis thaliana*) and maize (*Zea mays*), but that for *petA* operates specifically in Arabidopsis. Our study sheds light on the mechanisms by which RNA binding proteins cooperatively regulate mRNA stability and translation in chloroplasts.

INTRODUCTION

Chloroplasts were derived from a cyanobacterial ancestor through endosymbiosis (Martin et al., 1998; Timmis et al., 2004). However, in contrast with the genes of this cyanobacterial ancestor, the expression of most chloroplast genes is strongly influenced by posttranscriptional steps, including RNA splicing, editing, protein-mediated RNA stabilization, and translation activation (Stern et al., 2010; Barkan, 2011a; Manavski et al., 2018; Zoschke and Bock, 2018). Each of these steps requires nucleus-encoded RNA binding factors. Some of these factors are of eubacterial origin but have acquired new functions (Jenkins and Barkan, 2001; Till et al., 2001; Meurer et al., 2002; Chi et al., 2014), whereas most evolved later, during the coevolution of the nuclear and chloroplast genomes (reviewed in Barkan, 2011a). The functions of many such factors are largely conserved among land plant species (e.g., Barkan et al., 1994; Fisk et al., 1999; Jenkins and Barkan, 2001; Till et al., 2001; Ostheimer et al., 2003; Schmitz-Linneweber et al., 2005; Asakura and Barkan, 2006; Sun et al., 2013; Ferrari et al., 2017).

Chloroplast genes of vascular plants are typically organized in polycistronic transcription units, many of which give rise to transcripts that are processed in various ways and/or require translational activators for their expression. Many nucleus-encoded, gene-specific factors involved in these processes have been identified (as reviewed by Barkan and Goldschmidt-Clermont, 2000; Zerges, 2000; Barkan, 2011a; Germain et al., 2013; Zoschke and Bock, 2018). Many of these gene-specific factors are helical-repeat proteins, such as pentatricopeptide repeat (PPR), octatricopeptide repeat, and half-a-TPR proteins,

[1] These authors contributed equally to this work.
[2] Current address: Centre National de la Recherche Scientifique (CNRS), Institut de Biologie Moléculaire des 5 Plantes, 12 rue du Général Zimmer, 67084 Strasbourg, France.
[3] Address correspondence to chiweimr@ibcas.ac.cn.
The author responsible for distribution of materials integral to the findings presented in this article in accordance with the policy described in the Instructions for Authors (www.plantcell.org) is: Wei Chi (chiweimr@ibcas.ac.cn).
www.plantcell.org/cgi/doi/10.1105/tpc.18.00946

IN A NUTSHELL

Background: RNA folding, which underlies the formation of RNA structure, is important for the functions and regulation of RNAs in all living organisms. RNA chaperone proteins have evolved to assist in the (re)folding of RNA molecules. As a rather independent organelle, the plant chloroplast generates RNA molecules using its own gene expression system. However, our knowledge of RNA chaperone(s) inside chloroplasts is poorly understood.

Question: We set out to determine whether plant chloroplasts contain RNA chaperone protein(s), and if so, their roles in RNA metabolism in chloroplasts.

Findings: We isolated an RNA chaperone-like protein localized to the chloroplasts of Arabidopsis using a genetic method. Like many RNA chaperones, BSF (*petB/petD* Stabilizing Factor) shows nucleic-acid-melting activity, and its absence induces structural changes in RNA. Using various biochemical approaches, we found that BSF is associated with several chloroplast mRNAs. Further study showed that BSF indeed unfolds the structures of these RNAs to facilitate the binding of CRP1 (CHLOROPLAST RNA PROCESSING1), another important factor in chloroplast gene expression. In addition, we found that the RNA-binding protein PrfB3 can promote the RNA binding ability of BSF, suggesting that the function of BSF also requires the assistance of other RNA-binding proteins. Overall, our study uncovered an RNA-chaperon-like factor in plant chloroplasts and revealed its important role in chloroplast gene expression.

Next steps: Our findings raise multiple questions. Does BSF support the functions of other RNA-binding factors as an RNA chaperone-like protein? How does PrfB3 promote the RNA-binding ability of BSF? It would also be highly interesting to study the involvement of the relationship between CRP1 and PrfB3 in chloroplast gene expression.

whose modes of action have been a subject of great interest in recent years (Barkan and Small, 2014; Hammani et al., 2014; Wang et al., 2015). Some such proteins associate with the 5′ untranslated regions (UTRs) of chloroplast genes and simultaneously block 5′-3′ RNA degradation and enhance translation (e.g., Prikryl et al., 2011; Hammani et al., 2012). These findings have clarified the relationship between mRNA processing, stabilization, and translation activation.

Although many proteins bind to chloroplast RNA targets in a sequence-specific manner, they do not always act independently. In fact, in several cases, two or more RNA binding factors cooperate in the processing, stabilization, and/or translation of a single chloroplast mRNA. The RNA stability factor NAC2 and the RNA binding protein RBP40 act on the 5′ UTR of *psbD* encoding the D2 subunit of phtosystem II (PSII) and are required for its stability and translation activation (Schwarz et al., 2007). The stabilization factor MCA1 and the translation activator TCA1 form a large complex required for the efficient expression of *photosynthetic electron transfer A* (*petA*; Boulouis et al., 2011). Both the PRR proteins Proton Gradient Regulation 3 (PGR3) and ATP4/Suppressor of Variegation 7 (SVR7) are required to stabilize the 3′ end downstream of *ribosomal protein l14* (Rojas et al., 2018). In addition, some of these proteins might physically interact independently of their RNA targets, which increases the complexity of the RNA-protein interactome in chloroplasts. Nevertheless, the physiological significance and mechanism underlying this cooperation are still unknown.

Here, we describe the role played by an S1-domain-containing RNA binding protein, BSF (*petB/petD* Stabilizing Factor), in chloroplast gene expression in Arabidopsis (*Arabidopsis thaliana*). We show that BSF is required for the accumulation of the cytochrome b_6f (Cyt b_6f) complex due to its action on three chloroplast mRNAs encoding subunits of this complex: *petB*, *petD*, and *petA*. BSF associates with *petB*, *petD*, and *petA* mRNAs and stabilizes specific processed *petB* and *petD* RNA isoforms while also increasing the translational efficiency of *petD* and *petA*. Furthermore, BSF physically interacts with Peptide chain Release Factor 3 (PrfB3), a ribosomal release factor-derived protein (Stoppel et al., 2011) and the Arabidopsis PPR protein Chloroplast RNA Processing 1 (CRP1; Barkan et al., 1994; Fisk et al., 1999; Ferrari et al., 2017), whose RNA targets and effects on chloroplast gene expression overlap with those of BSF. Our results suggest that BSF and PrfB3 form an RNA chaperone machinery to support the function of CRP1. Analysis of the BSF ortholog in maize (*Zea mays*), RBCL RNA S1 BINDING DOMAIN protein (RLSB, referred to here as Zm-BSF), showed that a subset of these functions are conserved in maize.

RESULTS

The *bsf* Mutants Show Reduced Cyt b_6f Accumulation

By screening Arabidopsis T-DNA insertion lines for a *high chlorophyll fluorescence* phenotype (Meurer et al., 1996; Chi et al., 2008), we identified two pale-green mutants, *bsf-1* and *bsf-2*. Sequencing the PCR-amplified T-DNA–flanking regions revealed that the T-DNAs were inserted in the first intron and seventh exon of *AT1G71720*, respectively (Figure 1A). Both mutants failed to grow photoautotrophically. When grown on Suc-supplemented Murashige and Skoog (MS) medium, the mutants showed retarded growth and exhibited a pale phenotype compared with the wild type (Col-0; Figure 1B). The ratio of variable to maximum fluorescence (F_v/F_m), which reflects the maximum photochemical efficiency of PSII, was significantly lower in the *bsf* mutants than in the wild type (Figure 1B). Nevertheless, the F_v/F_m value was partially recovered in 20-d-old versus 10-d-old seedlings, especially in younger tissues (Figure 1B).

RT-PCR analysis showed that BSF was expressed in wild-type plants, but not in the bsf mutants (Supplemental Figure 1A). We

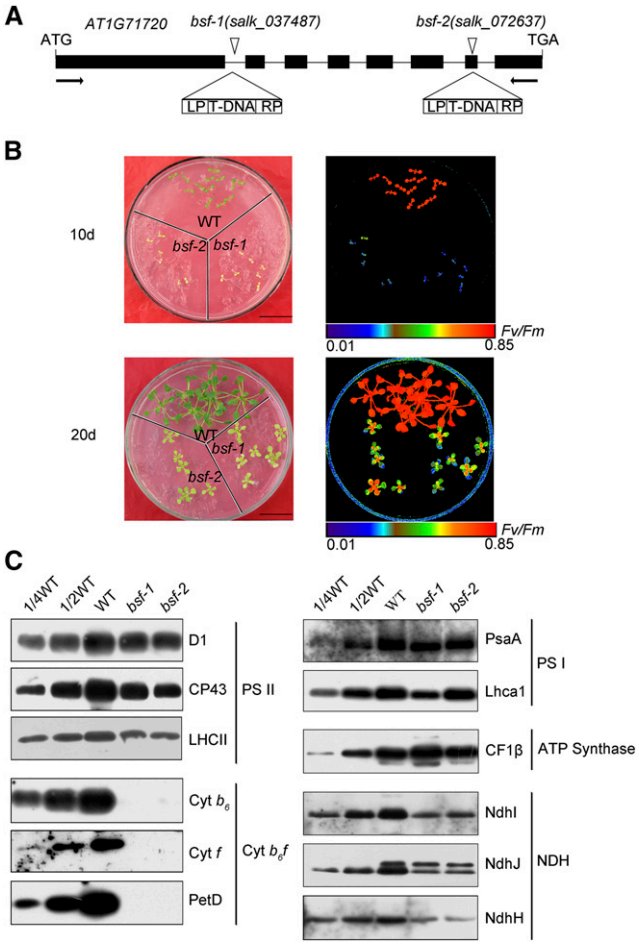

Figure 1. Identification and Phenotypes of *bsf* Mutants.

(A) Positions of the T-DNA insertions in *BSF*. Exons are indicated by black rectangles, introns by black lines, and T-DNA insertions by triangles. The name of the mutant allele is shown above each insertion. The T-DNA insertion in *bsf-1* is located in the first intron and that of *bsf-2* is located in the seventh exon of *AT1G71720*.

(B) Phenotypes and chlorophyll fluorescence ratios (F_v to F_m) of *bsf* and wild-type (WT) plants. Arabidopsis seedlings were grown on MS medium for 10 and 20 d. Chlorophyll fluorescence images are shown using the pseudocolor index below the figure.

(C) Immunoblot analysis of thylakoid membrane protein complexes from *bsf* and wild-type plants. Total protein (20 μg or the indicated dilution of wild-type samples) from 20-d-old plants was used for the analysis. The samples were separated by SDS-PAGE, transferred onto nitrocellulose membranes, and immunodecorated with the indicated antibodies raised against subunits of the PSII, photosystem I, Cyt b_6f, ATP synthase, and NDH complexes. CP43, the subunit of PSII reaction center; LHCII, the light harvesting protein of PSII; petD, the subunit IV of Cyt b_6f.

raised a polyclonal antibody against recombinant BSF protein (lacking the 63 N-terminal amino acid residues comprising the putative signal peptide). These antibodies detected a protein of the expected size of BSF in leaf extracts from wild-type plants (Supplemental Figure 1B). This protein was barely detected in leaf extracts from bsf plants (Supplemental Figure 1C), indicating that this protein was indeed BSF and that it was absent in both bsf mutants. Expression of the full-length *BSF* cDNA under the control of the constitutive 35S promoter fully restored the wild-type phenotype of *bsf-1* (Supplemental Figure 2), indicating that the disruption of *BSF* (*AT1G71720*) is responsible for the *bsf* phenotype.

BSF is predicted to be an RNA binding protein, as it harbors two S1 RNA binding domains. Therefore, it seemed likely that the pale phenotype and decline in F_v/F_m value resulted from reduced expression of chloroplast genes encoding components of the photosynthetic apparatus. To explore this possibility, we measured the abundance of representative subunits of distinct thylakoid membrane complexes in the mutants via immunoblot analysis of leaf extracts (Figure 1C). When compared with the wild type, in the *bsf* mutants the levels of Cyt b_6f complex subunits Cyt b_6, Cyt *f*, and subunit IV were drastically reduced, whereas the levels of PSII, photosystem I, and ATP synthase subunits were only slightly reduced or unchanged. These results indicate that BSF is involved in the accumulation of the Cyt b_6f complex. In addition to the Cyt b_6f complex, the levels of several subunits of the chloroplast NADH dehydrogenase-like (NDH) complex were also considerably reduced in *bsf* plants (Figure 1C).

Accumulation of 3′ Processed *petB* Transcripts and Monocistronic *petD* mRNAs is Affected in the *bsf* Mutants

One possible reason for the decrease in Cyt b_6f levels in the *bsf* mutants is defective accumulation of mRNAs encoding subunits of this complex. The Cyt b_6f complex core subunits Cyt f, Cyt b_6, and subunit IV are encoded by the plastid genes *petA*, *petB*, and *petD*, respectively. RNA gel blot analysis showed that *petA* transcripts were similar in size and abundance in the *bsf* mutant and the wild type, although the level of a minor monocistronic transcript may have been reduced slightly in *bsf* (Supplemental Figure 3). However, the population of *petB* transcripts clearly differed between the wild type and mutant (Figure 2). *PetB* is transcribed as part of the polycistronic transcription unit *psbB-psbT-psbH-petB-petD*. Approximately 20 distinct mono-, di-, and oligocistronic transcript species are produced during post-transcriptional processing of the *psbB* transcription unit (Stoppel and Meurer, 2013). RNA gel blot analysis conducted with eight probes (a–h) covering all coding and intergenic regions of this transcription unit showed that the levels of most transcripts were not altered in the *bsf* mutants (Figure 2, probes a, b, d, f, g, and h). However, several differences between the wild type and mutant transcript populations were apparent. First, the levels of some intron-containing transcripts were slightly or moderately higher in the *bsf* mutants (Transcripts 4 and 5). Second, a transcript that migrated slightly more slowly than Transcript 4 was detected specifically in the mutants using probes d and h. The most striking changes were the near absence of transcripts with 3′ ends in the *petB-petD* intercistronic region: the monocistronic *petB* transcript (Transcript 10) and dicistronic *psbH-petB* transcripts (Transcript 9; Figure 2, probes c and e).

Unlike the case in monocots (Barkan et al., 1994), very little monocistronic *petD* mRNA accumulates in Arabidopsis (Meierhoff et al., 2003), and it is difficult to detect by RNA gel blot analysis (as shown in Figure 2). To investigate the accumulation of monocistronic

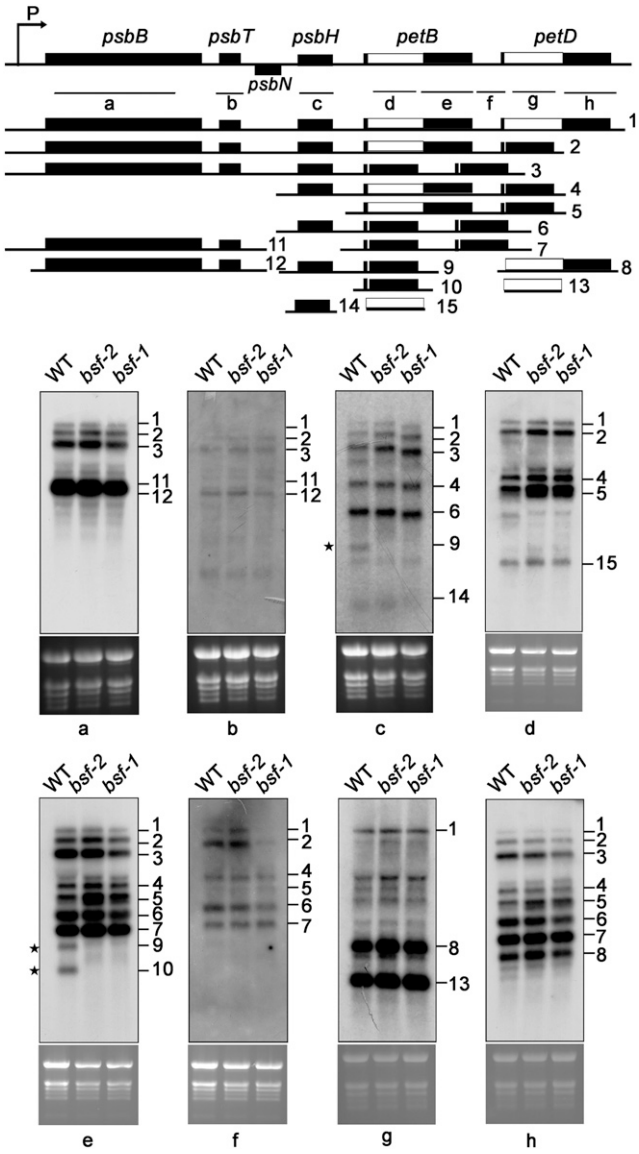

Figure 2. RNA Gel Blot Analysis of the *psbB-psbT-psbH-petB-petD* Transcription Unit in Wild-Type (WT) and *bsf* Plants.

A schematic representation of the *psbB-psbT-psbH-petB-petD* transcription unit is shown at the top. Probes (a–h) used in the RNA gel blot analysis are shown below as black lines. The precursor transcript and the most prominent processed and spliced products are displayed with their approximate lengths and numbered from 1 to 15. Total RNA (10 μg) was hybridized with the probes indicated at the bottom of the top panels. Ethidium-bromide-stained rRNA is shown below the blots as a loading control. *Transcripts that were absent from *bsf* plants.

petD transcripts, we performed a primer extension assay using a *petD*-specific oligonucleotide that binds close to the 5′ processed end (Supplemental Figure 4A). This oligonucleotide covered the first exon (7 nucleotides) and a fragment of the 5′ UTR of *petD* (17 nucleotides), yielding a 31- nucleotide extension product (Supplemental Figure 4A). When compared with the wild type, in *bsf* plants the levels of 5′-end-processed *petD* transcripts were slightly reduced (Supplemental Figure 4B). Our results localized the 5′ end of processed *petD* to a region 24 nucleotides upstream of the start codon; this finding differs slightly from results of a previous assay of the 5′ end of *petD* using circular-RT-PCR (31 nucleotides upstream of the start codon; Stoppel et al., 2011). This difference might result from differences in the experimental setup, as circular-RT-PCR requires additional steps, such as ligation and amplification. In any case, the processed 5′ end upstream of *petD* in maize maps much farther upstream, i.e., −144 nucleotides upstream from the start codon, corresponding with the 5′ end of the putative CRP1 footprint (Barkan et al., 1994; Zhelyazkova et al., 2012).

To clarify the nature of these RNA metabolism defects, we performed ribonuclease protection assays using four distinct probes (Supplemental Figure 5). Experiments using probes spanning the *psbH-petB* intergenic region as well as the 3′ splice junctions of *petB* and *petD* introns demonstrated that the intergenic processing of *psbH-petB* and the splicing of the *petD* and *petB* introns were not affected in *bsf* plants. However, 3′ processed petB transcripts, which are expected to give rise to a 148-base fragment, were barely detected in the mutants (Supplemental Figure 5), suggesting that processing and/or stabilization of the 3′ terminus of petB was affected in bsf.

BSF Is Required for the Translation of *petA* and *petD*

The changes in *petB*, *psbH-petB*, and *petD* transcript populations seemed insufficient to explain the severe deficiency in Cyt b_6f complex levels in the *bsf* mutants, as the mutants contained wild-type levels of most polycistronic *petB*/*petD*-containing transcript isoforms (Transcripts 1–7 in Figure 2), which also serve as efficient translation templates (Barkan, 1988; Zoschke et al., 2013). Thus, we reasoned that BSF might play additional roles in the translation of one or more of its RNA targets. To test this possibility, we analyzed the ribosome occupancy of all chloroplast genes using a ribosome-profiling (ribosome sequencing [Ribo-seq]) assay. This method uses deep sequencing to map mRNA fragments that are protected by ribosomes from ribonuclease attack, thus providing a genome-wide, quantitative readout of mRNA sequences bound by ribosomes in vivo (Ingolia, 2016).

We compared the ratios of normalized ribosome footprints mapping to each chloroplast gene in the wild type relative to bsf, as shown in Figure 3. The results revealed a severe defect in *petA* expression in the *bsf* mutant. Together with the finding that *petA* mRNA accumulates to near normal levels in *bsf* (Supplemental Figure 3), this finding indicates that BSF is required for *petA* translation. We also detected a weaker but clear defect in *petD* expression. These results indicate that defects in *petA* and *petD* translation account for the absence of the Cyt b_6f complex in *bsf* mutants. Interestingly, Ribo-seq revealed a clear defect in the expression of encoding subunit D of the NDH complex (*ndhD*) as well (Figure 3), suggesting that *ndhD* might be also a target of BSF. RNA gel blot analysis of *ndhD* transcripts in *bsf* (Supplemental Figure 3) showed that the level of encoding PS I subunit VII (*psaC*)-*ndhD* dicistronic transcripts was reduced slightly, whereas levels of other *ndhD* species (including monocistronic *ndhD*) were increased in *bsf* compared with the wild type. Nevertheless, the *ndhD* RNA pattern was not altered in *bsf*. The defect in *ndhD*

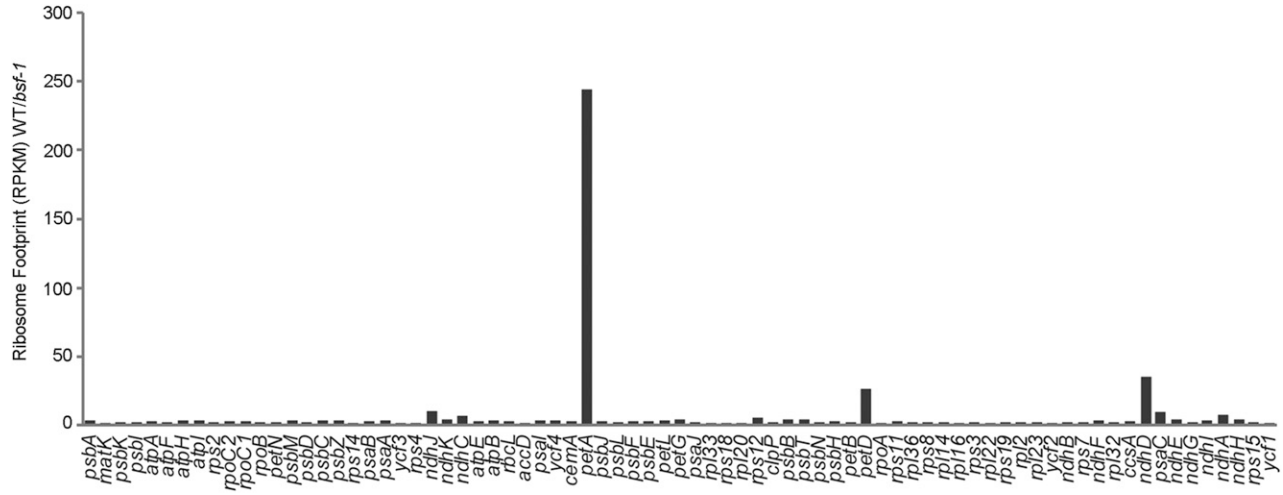

Figure 3. Analysis of Chloroplast mRNA Translation in the *bsf-1* Mutant by Ribosome Profiling.

Ribosome footprints from seedling leaves of the wild type (WT) and *bsf* mutant obtained by deep sequencing. Read counts were normalized to the total number of reads mapping to chloroplast ORFs. The values shown are the ratio of normalized read counts for each gene in the wild type vs the *bsf* mutant. RPKM, Reads Per Kilobase per Million mapped reads.

expression may be the cause of the reduced NDH complex levels in *bsf* plants (Figure 1C).

BSF Associates with *petB-petD*, *petA*, and Several Other Chloroplast RNAs in Vivo

Several chloroplast-targeting prediction algorithms (TargetP, ChloroP, and Predotar) identified a chloroplast transit peptide at the N terminus of the BSF protein sequence, and BSF has been detected during proteome analyses of the chloroplast nucleoid (http://ppdb.tc.cornell.edu/dbsearch/gene.aspx?acc=AT1G71720.1; Huang et al., 2013). As expected, a BSF-green fluorescent protein (GFP) fusion protein indeed localized to the chloroplast in Arabidopsis protoplasts (Supplemental Figure 6A). Immunoblot analysis of the thylakoid, envelope, and stromal fractions obtained from intact chloroplasts indicated that BSF localizes to the chloroplast stroma (Supplemental Figure 6B). Like many factors involved in chloroplast gene expression, the expression of BSF is induced by light, as BSF levels increased gradually during the greening of etiolated seedlings (Supplemental Figure 6C).

BSF contains two adjacent ribosomal protein S1-like domains at its C terminus. This RNA binding domain was first identified in ribosomal protein S1 but has since been found in diverse RNA binding proteins in all kingdoms of life (Régnier et al., 1987; Company et al., 1991; Gribskov, 1992; Langer et al., 1994). The presence of the S1 domains, along with the *petB* mRNA defects observed in the *bsf* mutants, suggests that BSF might be able to bind RNA. Therefore, we performed an RNA immunoprecipitation (RIP) assay to identify potential RNA targets. We performed RIP sequencing (RIP-seq) using chloroplast stroma with BSF-specific antibodies and preimmune serum as a control (Figure 4A; Supplemental Data Set 1). As shown in Figure 4A, the most highly enriched sequences in the RIP-seq experiment mapped to the *petB* and *petD* loci, as revealed in two replicate experiments. A closer look at the sequencing data revealed that the highest levels of enrichment occurred in the *petB-petD* intergenic region and the 3′ end of the *petD* coding region (Supplemental Figure 7). In addition to *petB* and *petD*, the 5′ UTR of *petA* was also highly enriched in our RIP-seq experiment (Figure 4A; Supplemental Figure 7). These RIP-seq data are in accordance with the expression defects of *petA*, *petD*, and *petB* in the *bsf* mutant.

We also detected the enrichment of encoding Cytochrome b559 of PS II (*psbE*), encoding subunit J of PS I (*psaJ*)-*Ribosomal Protein L33* (rpl33), and encoding NDH subunit 4L (*ndhE*) in the RIP-seq experiment (Figure 4A). Slot-blot hybridization of immunoprecipitated RNAs validated the enrichment of all RNAs found to be targets of BSF (Figure 4B). A previous study showed that the maize BSF ortholog, RLSB, associates with *rbcL* (Bowman et al., 2013); however, when compared with the other targets, *rbcL* exhibited only slight enrichment in our RIP-seq experiment. A previous study showed that BSF binds to *hypothetical chloroplast open reading frame 1* (*ycf1*) mRNA (Yang et al., 2016), but no association between BSF and *ycf1* was observed in our RIP-seq analysis.

The results detailed above suggest that BSF targets other RNAs in addition to *petB*, *petD*, and *petA*. Therefore, we investigated whether the transcript levels of these genes were also affected in *bsf*. Similar to *petA*, the RNA patterns of *psbE*, *psaJ*, *rpl33*, and *ndhE* were not substantially altered in *bsf*, although the levels of some RNA species were slightly reduced (Supplemental Figure 3), suggesting that BSF plays little, if any, role in the stability/processing of these mRNAs.

BSF Directly Interacts with PrfB3 and AtCRP1

In addition to BSF, the ribosomal release factor-derived PrfB3 protein is also required for the stability of 3′ processed *petB* transcripts in Arabidopsis (Stoppel et al., 2011). Furthermore, the PPR protein CRP1 associates with both *petA* and *petD* RNAs,

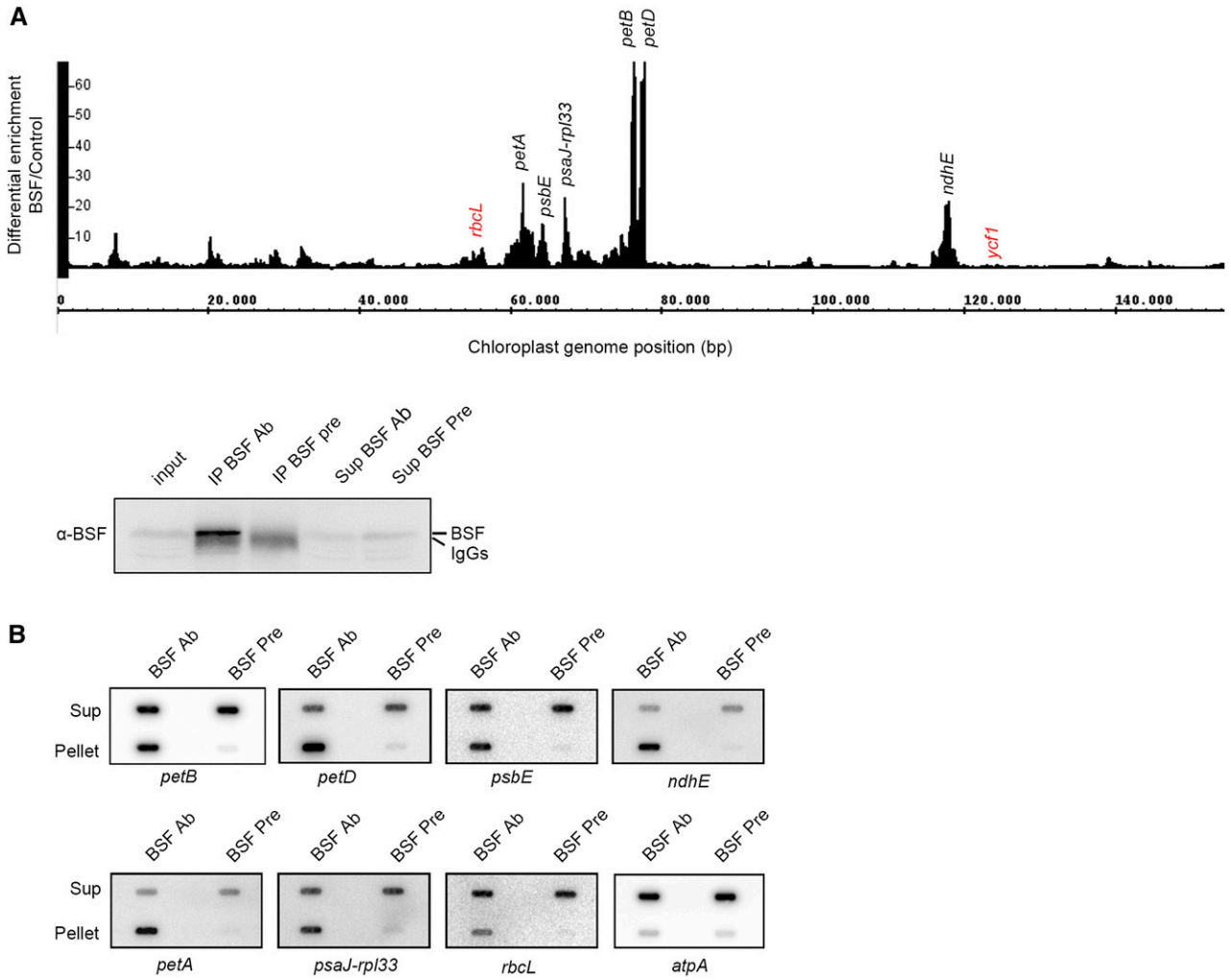

Figure 4. BSF Is Associated With Multiple RNA Targets In Vivo.

(A) RIP-seq analysis of BSF. RIP was performed with wild-type (WT) stromal extracts using BSF-specific antibodies (Ab) and preimmune (Pre) serum as a control. The success of the IP was tested by immunodetection using 30 μg of stromal extract as input, 1/10 of the IP, and 30 μg of the supernatants (Sup). RNAs in the pellets were subjected to RNA-seq analysis. The Integrative Genome Browser snapshot shows the ratio (differential enrichment) of BSF/control RPKM-normalized reads of the two replicates across the whole chloroplast genome. Genome positions are shown, and the most highly enriched RNA targets are indicated in black. Previously identified targets (*rbcL* and *ycf1*) are indicated in red.

(B) Slot-blot conformation of the RNA targets identified by RIP-seq analysis. RIP was performed as described above, and 1/3 of the pellet RNA and 1/20 of the supernatants were used for slot-blot analysis. Specific probes for the target RNAs are indicated. The *atpA* probe was used as a negative control.

stimulating their translation in maize and Arabidopsis (Barkan et al., 1994; Fisk et al., 1999; Schmitz-Linneweber et al., 2005; Zoschke et al., 2013; Ferrari et al., 2017). The RNA targets of these proteins and their effects on chloroplast gene expression overlap with those of BSF. To determine whether these proteins interact directly, we performed in vitro pull-down assays using purified recombinant proteins expressed in *Escherichia coli* (Figure 5A). Both maltose binding protein (MBP)–tagged PrfB3 and MBP-AtCRP1 fusion proteins bound to amylose resin pulled down recombinant glutathione *S*-transferase (GST)–tagged BSF, but MBP alone did not. As a control, we used another PPR protein, Early Chloroplast Development 1 (ECD1; Jiang et al., 2018) , which failed to pull down recombinant BSF in the same assay, suggesting that the interaction between AtCRP1 and BSF is specific. These interactions were further verified using the yeast two-hybrid system (Figure 5B). Yeast cells coexpressing BSF and either PrfB3 or AtCRP1 grew normally on synthetic complete medium lacking Trp, Leu, and His and supplemented with 5-bromo-4-chloro-3-indolyl α-D-galactopyranoside (X-α-Gal), suggesting that BSF interacts with PrfB3 and AtCRP1 in yeast cells. This evidence suggests that AtCRP1 and PrfB3 can interact physically with BSF.

To validate these interactions in vivo, we performed coimmunoprecipitation analysis using total proteins from wild-type Arabidopsis leaf tissue. Immunoprecipitations were performed with preserum (Pre), anti-ECD1 serum, and anti-PrfB3 serum, and the

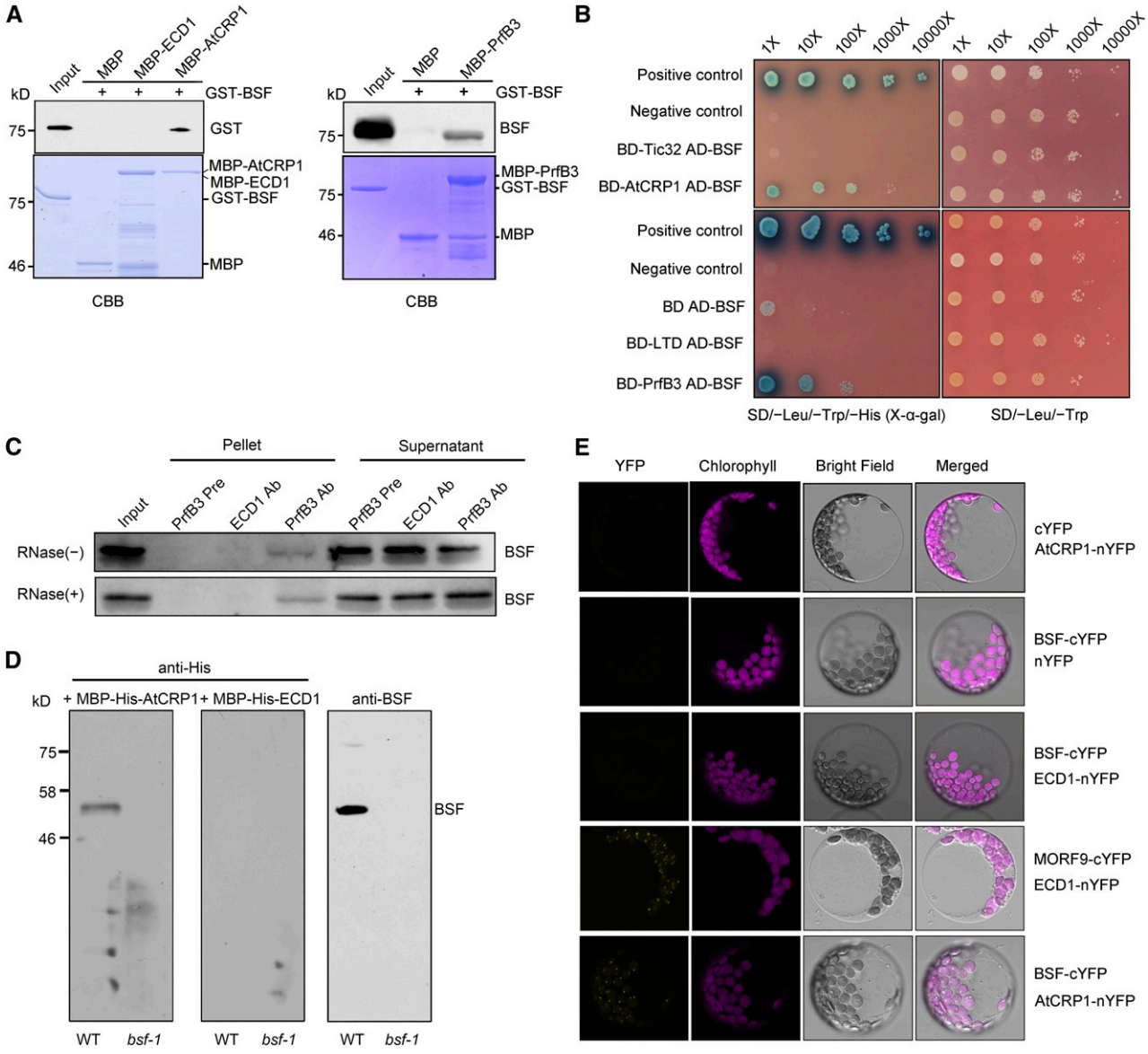

Figure 5. BSF Directly Interacts With AtCRP1 or PrfB3.

(A) Pull-down assay of BSF and AtCRP1 or PrfB3. Full-length GST-tagged BSF was used as prey. MBP-tagged AtCRP1 and PrfB3 were used as baits. Purified recombinant proteins were bound to amylose resin, and the bound proteins were eluted and analyzed by immunoblotting or CBB (Coomassie Brilliant Blue G-250) staining. MBP alone and MBP-tagged ECD1, another PPR protein (Jiang et al., 2018), were used as the control baits. Input: 4% of the prey protein.

(B) Yeast two-hybrid analysis of the interaction between BSF and AtCRP1 or PrfB3. Mature PrfB3 and AtCRP1 proteins were fused to the GAL4 DNA binding domain (BD-PrfB3, BD-AtCRP1), whereas mature BSF protein was fused to the GAL4 activation domain (AD-BSF). AD-LTD (Ouyang et al., 2011) and AD-Tic32 were used as negative controls.

(C) Coimmunoprecipitation of BSF with PrfB3. Total protein extracts (untreated or treated with RNase) were subjected to immunoprecipitation with PrfB3 antibodies, and the presence of BSF in the immunoprecipitated pellets was tested by immunoblotting with BSF antibodies. Immunoprecipitation with preserum (Pre) and ECD1 antibody served as negative controls. The supernatants obtained from coimmunoprecipitation were also subjected to immunoblotting as controls. Input: 1/8 IP (immunoprecipitation).

(D) Overlay assay of the BSF-AtCRP1 interaction. Overlay of His-MBP-tagged AtCRP1 and ECD1 proteins on total proteins from the wild type (WT) and *bsf* was performed, followed by immunoblot analysis with anti-His or BSF antibody.

(E) BiFC assay of the interaction between BSF and AtCRP1. Plasmids encoding fusion constructs with the N- or C-terminal parts of YFP (BSF-cYFP and AtCRP1-nYFP, respectively) were transiently expressed in Arabidopsis protoplasts. Yellow signals indicate YFP fluorescence; magenta signals indicate chloroplast autofluorescence. The cotransformation of ECD1-nYFP and BSF-cYFP was used as a negative control. The interaction between ECD1 and MORF9 in nucleoids (Jiang et al., 2018) is also shown as a positive control.

presence of BSF was determined in the pellet and supernatant by immunoblotting with BSF antibodies. The results clearly showed that PrfB3 coimmunoprecipitated with BSF, whereas ECD1 did not (Figure 5C). Moreover, when RNA was eliminated from the extracts via RNase I treatment (Supplemental Figure 8), PrfB3 was still immunoprecipitated by BSF, suggesting that the association between BSF and PrfB3 does not depend on RNA.

Because no antibody against AtCRP1 is currently available, we performed a protein overlay assay to detect a BSF-AtCRP1 interaction using total proteins from wild-type plants. BSF interacted with AtCRP1 but not ECD1 (Figure 5D). In addition, Bimolecular Fluoescence Complementation (BiFC) experiments confirmed that AtCRP1 and BSF are located in close proximity in Arabidopsis protoplasts (Figure 5E), suggesting that AtCRP1 and BSF interact in planta. It should be noted that the fluorescent signals generated with the combination of AtCRP1 and BSF displayed a punctuated pattern resembling the appearance of nucleoids (Powikrowska et al., 2014), which is in agreement with the identification of AtCRP1 and BSF as nucleoid-associated proteins (Huang et al., 2013; Ferrari et al., 2017). We could not detect the BSF-PrfB3 interaction by BiFC experiments in Arabidopsis protoplasts under conditions in which the AtCRP1-BSF interaction was unambiguous. This may be due to low stability and/or expression level of Yellow Fluoescence Protein (YFP)-fused PrfB3 protein in Arabidopsis protoplasts, but it is also possible that PrfB3 and BSF do not form sufficiently abundant or long-lived complexes for detection in this manner.

Because both AtCRP1 and PrfB3 physically interact with BSF, we reasoned that they might function as components of a common complex. To investigate this possibility, we performed Blue Native (BN)-PAGE using chloroplast stroma from Arabidopsis seedlings expressing FLAG-IgG-tagged AtCRP1 (Supplemental Figures 9 and 10). Our results indicated that all three proteins are present in a putative complex with a molecular mass of ~440 kD (Supplemental Figure 10), suggesting the existence of a complex involving AtCRP1, BSF, and PrfB3. PrfB3, but not AtCRP1, comigrated with BSF at other positions in the BN-PAGE (Supplemental Figure 10), suggesting that PrfB3 and BSF can also form complexes independent of AtCRP1.

To further elucidate the components of BSF-associated complexes, we took advantage of transgenic lines expressing FLAG-IgG-tagged BSF protein (Supplemental Figure 9) to perform immunoprecipitation with the FLAG antibody. Proteins copurified with BSF were eluted and subjected to mass spectrometry. Using transgenic lines expressing FLAG-IgG-tagged FtsHi1 protein (a AAA-ATPase of chloroplasts) and wild-type plants as two negative controls, we identified 23 chloroplast-localized proteins that coimmunoprecipitated with BSF in two independent replicates (Supplemental Table; Supplemental Data Set 2). These proteins were found in FLAG immunoprecipitates from *BSF-FLAG-IgG* transgenic lines but were absent in the negative controls. As expected, AtCRP1 was copurified with BSF, in accordance with a physical interaction between AtCRP1 and BSF. Interestingly, in addition to AtCRP1, three PPR proteins of unknown function were also identified in this assay, suggesting that BSF might have multiple PPR protein partners in vivo (Supplemental Table). Surprisingly, the mass spectrometry analysis did not detect PrfB3 protein in FLAG immunoprecipitates from *BSF-FLAG-IgG* transgenic lines. However, immunoblotting of the same immunoprecipitation sample subjected to mass spectrometry detected PrfB3 (Supplemental Figure 11), indicating that PrfB3 coimmunoprecipitated with BSF but was not detected by the mass spectrometry method used in this study. Some specific proteins (e.g., TIC20-I, a protein of translocon complex of the inner envelop memebrane of chloroplasts) are extremely difficult to detect by mass spectrometry but can be detected clearly by immunoblotting (Kikuchi et al., 2018).

BSF Binds to RNAs in Vitro

To investigate whether BSF directly binds to its main target RNAs, we performed electrophoretic mobility shift assays (EMSAs) using RNA probes derived from *petB*, *petD*, and *petA* (Figures 6 and 7). The RNA sequences used for these experiments were based on the most highly enriched regions in the RIP-seq data. As shown in Figure 6A, BSF bound to the region 1 to 35 nucleotides downstream of the *petB* translation termination site (probe a) and failed to recognize the other probes within the *petB-petD* intergenic region (probes b–e). This BSF binding site is adjacent to the putative AtCRP1 binding site, whose 3′ end coincides with the processed 3′ end downstream of *petB* (Stoppel et al., 2011). In addition, BSF bound to a probe covering the last 30 nucleotides of the coding region of *petD* (probe g; Figure 6A). This result is in agreement with the observation that the most highly enriched region, as determined by RIP-seq analysis, was found within 60 nucleotides upstream of the *petD* stop codon (Supplemental Figure 7). To confirm the binding specificity of BSF to its target RNAs, we performed an EMSA using unlabeled RNAs as competitors. Unlabeled probes a, g, and j competed with labeled probes in the binding assay (Supplemental Figure 12A), whereas poly(A), poly (U), poly(G), and poly(C) RNA oligonucleotides had no effect on the binding of BSF to the *petB* 3′ UTR (Supplemental Figure 12B).

EMSAs confirmed that recombinant PrfB3 binds specifically to the *petB* 3′ UTR and the 3′ coding region of *petD* (probes a and g in Supplemental Figure 13; Stoppel et al., 2011). To address how BSF and PrfB3 cooperatively affect RNA metabolism, we performed an EMSA using a low concentration of BSF and increasing concentrations of MBP-PrfB3 (Figure 6B). No shifted RNA band was present when a low concentration of BSF or MBP-PrfB3 protein alone was used (100 nM BSF or 150 nM MBP-PrfB3). However, the combination of both proteins at the same concentration produced a clear BSF-RNA complex but did not produce a MBP-PrfB3-RNA complex or a supercomplex containing both BSF and MBP-PrfB3. In addition, the levels of this complex increased with increasing amounts of MBP-PrfB3 protein and constant amounts of BSF, suggesting that MBP-PrfB3 considerably increases the RNA binding ability of BSF. Furthermore, at higher concentrations (800 nM), PrfB3 bound to probe a (3′ UTR of *petB*) in the absence of BSF (Figure 6B). The EMSA pattern of the PrfB3-RNA complex in this study seemed to be somewhat different from that reported by Stoppel et al. (2011): Instead of one PrfB3-RNA complex as seen in our study, two complexes were observed in previous EMSA assays. This distinct binding pattern of PrfB3 might be due to the different lengths of the *petB* 3′ UTR probe (35 vs. 70 nucleotides) and/or different forms of

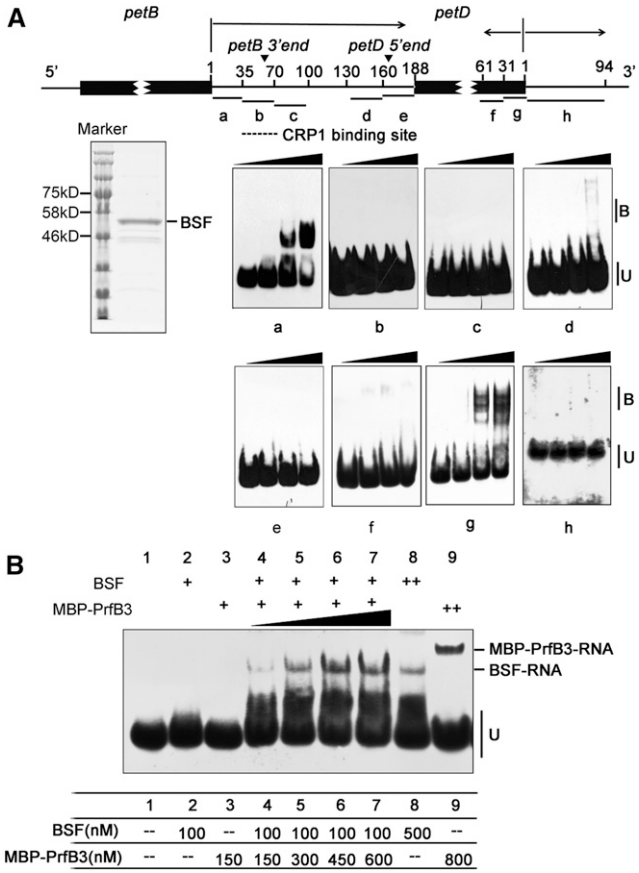

Figure 6. BSF Binds to the *petB-petD* Intergenic Region and the 3′ End of *petD* In Vitro.

(A) EMSA using recombinant BSF and RNAs derived from *petB-petD*. The diagram shows the positions of the RNA oligonucleotide probes (black lines labeled a–h) within *petB* and *petD*. The coding regions of *petB* and *petD* are indicated by black rectangles. The arrowheads show the positions of the native *petB* 3′ end and *petD* 5′ end. The putative AtCRP1 binding site is indicated by a dotted line. The substrates were mixed with increasing concentrations of BSF (125, 250, and 500 nM). Protein-bound **(B)** and unbound RNAs **(U)** are indicated. A Coomassie blue-stained SDS-PAGE gel containing purified BSF protein is shown on the left.

(B) EMSA with BSF in combination of MBP-PrfB3. The amounts of proteins used in each lane are shown in the table below. Probe **(A)** at 500 pM was used in all reactions.

recombinant proteins (MBP-PrfB3 vs. His-PrfB3) used in the two studies. It is likely that the PrfB3-RNA complex observed in our assay corresponds to the more abundant higher mobility complex, which might represent the more stable complex (Stoppel et al., 2011). Adding MBP had no impact on the RNA binding ability of BSF (Supplemental Figure 14), suggesting that PrfB3 plays a specific role in supporting the RNA binding ability of BSF.

The BSF binding site of *petA* was localized to a region 1 to 40 nucleotides upstream of the *petA* translation initiation codon (Figure 7A; Supplemental Figure 12), which is also in agreement with the strong enrichment of the *petA* 5′ UTR in the RIP-seq data (Supplemental Figure 7). Direct interaction with the *petA* 5′ UTR also has been reported for both CRP1 and AtCRP1 (Schmitz-Linneweber et al., 2005; Ferrari et al., 2017). Interestingly, the potential binding site of AtCRP1 also lies in this region (Ferrari et al., 2017). To further clarify the functional interplay between AtCRP1 and BSF, we pinpointed the site of BSF binding using EMSAs with a series of 15- nucleotide probes within this region (Figure 7B). This assay narrowed down the binding site of BSF to 6 to 20 nucleotides upstream of the *petA* translation initiation codon. The prediction by Mfold (http://unafold.rna.albany.edu/?q=mfold) showed that the BSF binding site forms a duplex with the putative AtCRP1 binding site (Figure 7C). Given that PPR proteins bind nucleic acids with a strong preference for single-stranded RNA relative to double-stranded RNA (Williams-Carrier et al., 2008), BSF binding in this region might affect the binding of the AtCRP1 protein to the *petA* 5′ UTR.

BSF Displays RNA Chaperone–Like Activity

The structure of the S1 domain is quite similar to that of cold shock proteins, which not only bind to RNA targets but also possess RNA chaperone activity (Weber and Marahiel, 2003; Phadtare, 2011; Duval et al., 2013). One example is the Cold shock protein A (CspA) family of cold shock proteins in *E. coli* (Jiang et al., 1997). Therefore, we performed two well-established RNA chaperone assays to determine whether BSF possesses RNA chaperone activity similar to that of CspA (Phadtare et al., 2002a; Kang et al., 2013). First, we evaluated the nucleic acid melting activity of BSF by measuring fluorescence arising from the melting of partially double-stranded DNA molecules (Figures 8A to 8C; Supplemental Data Set 3). As shown in Figure 8C, adding BSF protein to the reaction mixture produced strong fluorescent signals (~45% that of CspA, the positive control). As controls, when MBP, MBP-PrfB3, or MBP-ECD1 was added to the reaction mixture, extremely weak fluorescence was detected. Thus, BSF has clear nucleic acid melting activity in vitro. Given that PrfB3 stimulated RNA binding of BSF in vitro, we further measured the nucleic acid melting activity of BSF in combination with PrfB3. However, the nucleic acid melting activity of BSF was not obviously altered in the presence of PrfB3 (Supplemental Figure 15).

Second, we introduced BSF into *E. coli* BX04, a cold-stress–sensitive mutant that lacks four cold-shock proteins that function as RNA chaperones (Xia et al., 2001; Phadtare et al., 2002a; Yang et al., 2012), and investigated whether BSF would complement the mutant phenotype. As shown in Figure 8D, when grown at the normal growth temperature (37°C), BX04 cells harboring BSF, CspA, or the pINIII vector (as a negative control) grew normally. However, when the cells were incubated at a lower temperature (20°C), cells expressing BSF or CspA grew well, whereas cells harboring the pINIII vector did not. These results indicate that BSF can complement the cold-sensitive phenotype of *E. coli* BX04 cells, strongly suggesting that BSF possesses RNA chaperone activity.

If BSF acts as an RNA chaperone, we reasoned that its absence would affect RNA structure in vivo. We therefore investigated the RNA structure of the *petB* 3′ UTR in *bsf*, *prfB3*, and wild-type plants using an in vivo dimethyl sulfate (DMS) probing assay, as described previously (Meurer et al., 2017). DMS methylates the N1 and N3 position of unpaired adenines and cytosines, respectively,

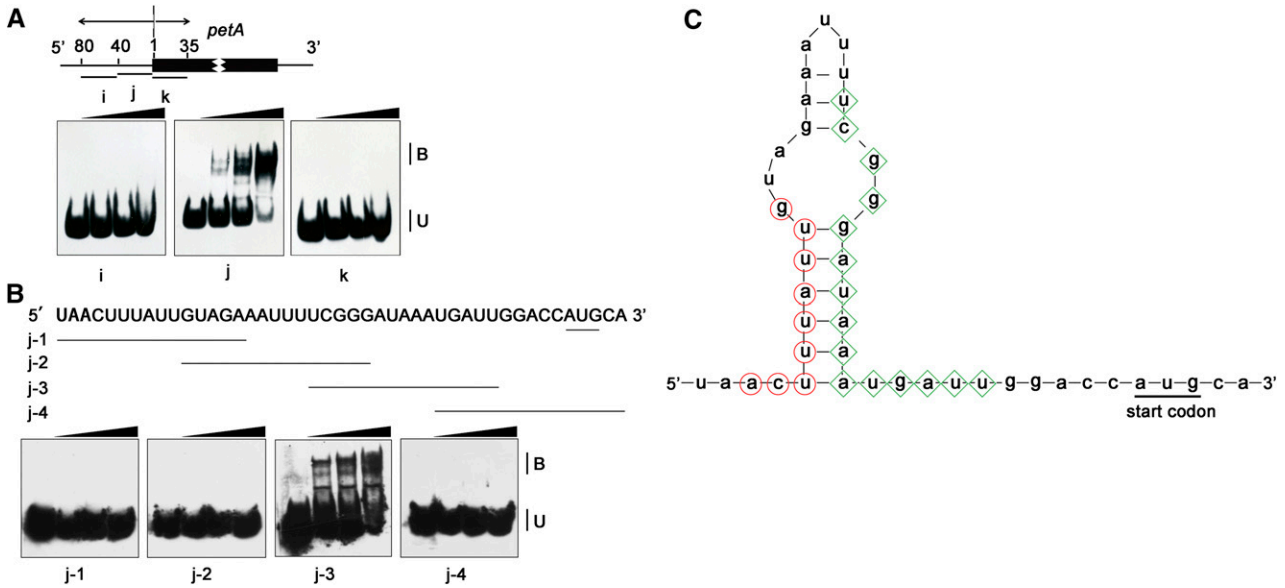

Figure 7. BSF Binds to the 5′ UTR of *petA* In Vitro.

(A) EMSA using recombinant BSF and RNAs derived from *petA*. Three probes covering the 5′ UTR and part of the 5′ coding region of *petA* were used. The positions of the RNA oligonucleotide probes (black lines labeled i–k) are shown in the top diagram. The experimental procedure was the same as that in Figure 6A.

(B) Fine-mapping the RNA binding sites of BSF in the *petA* 5′ UTR. Sequences and positions of four 15-nt oligonucleotide probes (from j-1 to j-4) are depicted at the top; the *petA* translation initiation site is underlined. The experimental procedure was the same as that in Figure 6A.

(C) Secondary structure of the *petA* 5′ UTR calculated with Mfold assuming a temperature of 30°C. Putative AtCRP1 binding sites based on the RIP experiment and in silico prediction (Ferrari et al., 2017) are indicated by red circles, and BSF binding sites are indicated by green diamonds. The *petA* translation initiation site is underlined.

leading to strong reverse transcription stops one base before the modified nucleotide (Lempereur et al., 1985). With use of this reagent, the secondary structure of RNA fragments is reflected by the products of primer extension. We isolated total RNA from DMS-treated plants and subjected it to a primer extension assay using a *petB* 3′ UTR-specific antisense oligonucleotide. The *petB* 3′ region was much more accessible to DMS, and thus less structured, in the wild type compared with *bsf* and *prfB3* (Figure 8E), indicating that the structural state of the *petB* 3′ region is dependent on the presence of BSF and PrfB3 in vivo.

The Role of BSF in *petD* Expression Is Conserved in Arabidopsis and Maize

BSF is highly conserved among land plants. A previous study suggested that RLSB (Zm-BSF) is a posttranscriptional regulator of *rbcL* mRNA (Bowman et al., 2013), which appears to be inconsistent with the role of BSF uncovered in this study. To clarify the function of Zm-BSF, we performed a ribosome profiling assay of the heteroallelic progeny of a complementation test cross between the same Zm-*bsf* mutant alleles used in the previous study (Zm-*bsf-1*/*-2*; Figure 9A). We plotted the data as the ratio of signal for each chloroplast gene in the wild type relative to the mutant (Figure 9A). The results revealed a clear defect in *petD* expression but no change in *rbcL* expression in the mutant. A minor decrease in *psbA* translation was also found, but this might have been a secondary effect of the Cyt b_6f deficiency, as a similar reduction in psbA translation has also been observed in several other mutants (Zoschke et al., 2013). RNA gel blot hybridizations showed that the pattern of *petD*-containing transcripts was identical in the *Zm-bsf* and *crp1* mutants (Figure 9B), indicating that the cooperative role of BSF and CRP1 in *petB*/*D* RNA metabolism is conserved in maize and Arabidopsis. However, the *petA* and *ndhD* translational defects observed in the Arabidopsis *bsf* mutants were not found in the maize mutant, indicating that only a subset of BSF functions are conserved in Arabidopsis and maize.

DISCUSSION

BSF Functions in Chloroplast Gene Expression

The S1 domain is structurally and functionally similar to the cold-shock domain; both domains assume an ancient β-barrel fold structure to bind nucleic acids (Bycroft et al., 1997). In some cases, the S1 and cold-shock domains also mediate the nucleic acid melting or annealing activity of the protein and thus remodel local RNA structures. Several S1-domain-containing proteins have been localized to chloroplasts (http://ppdb.tc.cornell.edu), but their functions remain largely unknown. In this study, we demonstrated that the S1-domain-containing BSF protein functions as an RNA chaperone–like factor in chloroplast gene expression and that it facilitates the activities of two previously described RNA binding proteins, CRP1 and PrfB3.

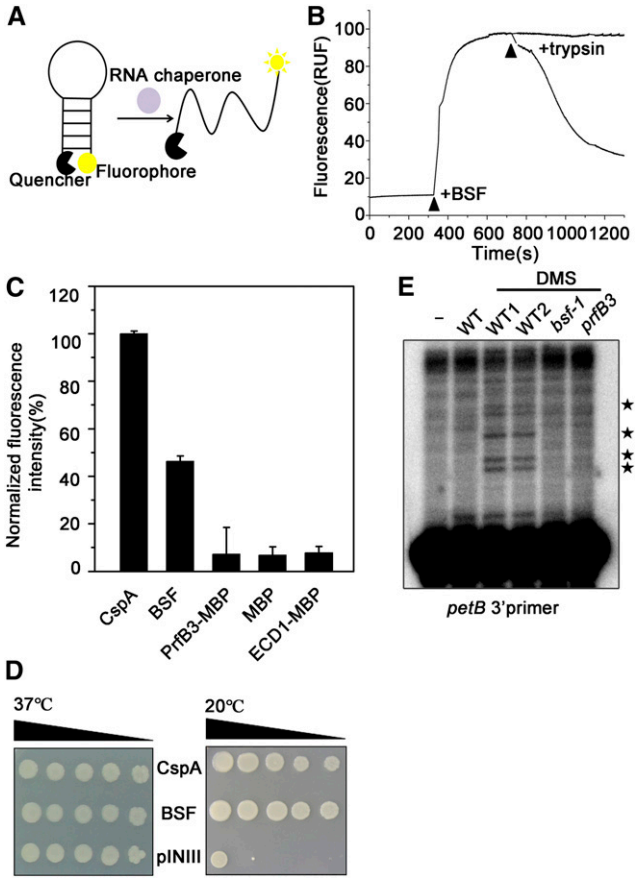

Figure 8. BSF Displays RNA Chaperone Activity.

(A) Nucleic acid-melting assay of BSF. The diagram shows the method used to measure nucleic acid melting activity in vitro: base pairing of nucleic acid molecules labeled with a fluorophore and quencher is broken by RNA chaperones, inducing fluorescence emission.

(B) The fluorescence of an 82-nucleotide molecular beacon monitored upon BSF addition. The excitation and emission wavelengths used were 555 and 575 nm, respectively. The effect of BSF removal was tested by adding trypsin in 50-fold excess to the reaction mixtures. The time points at which the respective proteins were added are indicated by arrows. RUF, Relative Fluorescence Unit. The data used to generate this graph are provided in Supplemental Data Set 3.

(C) The relative fluorescence obtained using each protein is shown (100% equals fluorescence obtained using CspA). The experiment was repeated three times. Data are means ± SD.

(D) Complementation ability of BSF in *E. coli* BX04 mutant cells. Diluted *E. coli* cell cultures expressing BSF, CspA (positive control), or pINIII vector (negative control) were spotted onto LB-agar plates, and the cells were incubated at 37°C or 20°C.

(E) Structural probing of the *petB* 3′ UTR using DMS. Two wild-type samples (WT1 and WT2), *bsf*, and *prfB3* were treated with DMS. Total RNA was isolated and subjected to a primer extension assay. RNA obtained from untreated wild-type plants was used as a negative control. The short primer extension bands occurring only in DMS-treated samples correspond to methylation events in unstructured or protein-free RNA fragments and are indicated by asterisks. The 5′ end of the primer was mapped 45 nucleotides downstream with respect to the termination codon of *petB*.

BSF appears to bind RNA targets in a sequence-specific manner. In this context, BSF also appears to act differently from classical RNA chaperones, which generally bind weakly to diverse RNA substrates with low sequence specificity (Doetsch et al., 2011). However, it should be noted that RNA binding specificity and RNA chaperone activity are not mutually exclusive. Such RNA chaperone–like factors have been reported in other organisms (e.g., Bokinsky et al., 2006; Paukstelis et al., 2008). According to the "pre-association" theory, such proteins assist RNA folding via sequential protein-RNA interactions (Bokinsky et al., 2006). First, nonspecific interactions occur rapidly, inducing large conformational fluctuations in RNA. Specific protein-RNA interactions then stabilize the native RNA structure (Herschlag, 1995; Bokinsky et al., 2006). This theory might explain the role of BSF in RNA binding and folding. It appears that BSF has evolved from ancient general nucleic acid binding proteins but has subsequently been recruited for interaction with specific transcripts and has acquired new functions during endosymbiosis. Similarly, the plant-specific PALE CRESS is thought to belong to a new class of RNA chaperones, as it induces proper 23S rRNA folding in vivo (Meurer et al., 2017).

Our RIP-seq analysis showed that BSF associates with *petB*, *petD*, and *petA* mRNAs in vivo (Figure 4). Furthermore, our RNA gel blot, ribonuclease protection, and ribosome profiling assays showed that BSF affects the stability and translation efficiency of these RNAs independently. The defect in accumulation of transcripts with processed 5′ and 3′ termini in the *petB-petD* intergenic region was originally described in *prfB3* and *crp1* mutants (Barkan et al., 1994; Fisk et al., 1999; Stoppel et al., 2011). The absence of RNAs with a processed 3′ end in the *petB-petD* intergenic region in the *bsf* mutants suggests that BSF, together with AtCRP1 and PrfB3, serves as a barrier to block 3′→5′ exoribonucleolytic attack, thereby protecting the 3′ end of *petB*. However, it appears that this process has little effect on *petB* protein output, as indicated by the ribosome profiling data. The arrangement of processed RNA termini in the *petB-petD* intergenic region strongly suggests that CRP1 in maize simultaneously stabilizes both 5′ and 3′ RNA termini via the canonical PPR roadblock mechanism (Barkan et al., 1994; Zhelyazkova et al., 2012). However, the situation is different in Arabidopsis, where very little monocistronic *petD* RNA accumulates, and its 5′ end maps well downstream of the presumed AtCRP1 binding site (Figure 6A). It is likely that BSF bound to the *petB-petD* intergenic region is important for binding of AtCRP1 downstream, where its primary function is to enhance *petD* translation. It seems possible that transient binding of BSF is sufficient to reduce secondary structure and allow AtCRP1 binding without impeding ribosome movement . Our RIP-seq and EMSA data suggest that BSF binds near the 3′ end of the *petD* open reading frame. This is puzzling given that ribosomes transit through this region.

In addition to *petB*, *petD*, and *petA*, BSF associates in vivo with three other RNA species: *psbE*, *psaJ-rpl33*, and *ndhE* (Figure 4). For the *psaJ*-containing operon, we found that the levels of some precursor RNAs were higher in *bsf* compared with the wild type, suggesting that BSF might participate in the processing of this polycistronic transcript (Supplemental Figure 3). This is also in accordance with the finding that BSF associates with the *psaJ-rpl33* intergenic region. Similarly, a possible role of BSF in

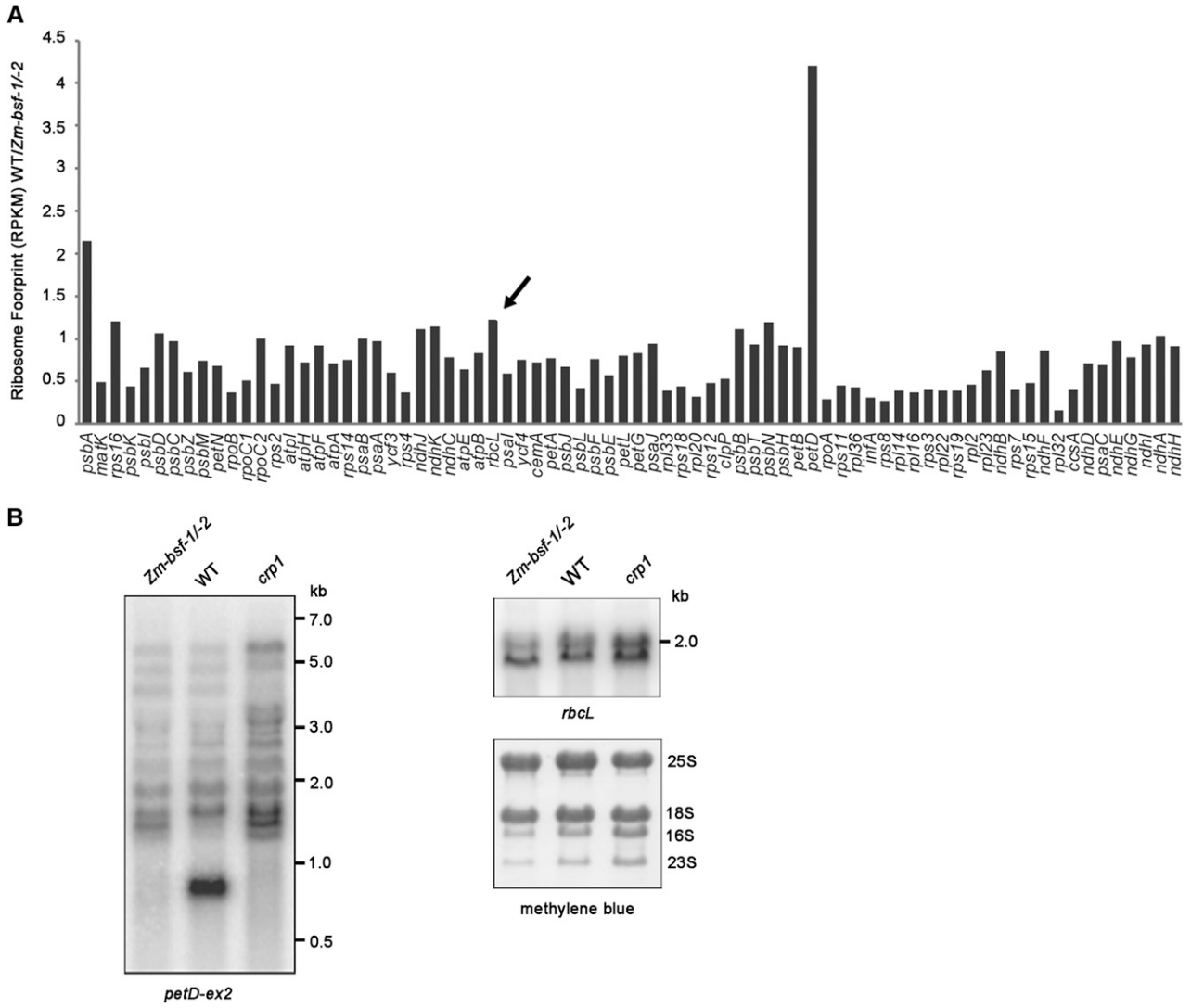

Figure 9. *petD* Expression Is Defective in the Maize Zm-*bsf-1/-2* Mutant.

(A) Analysis of chloroplast mRNA translation in Zm-*bsf-1/-2* mutants by ribosome profiling. The experimental procedure was the same as in Figure 3 except that maize seedlings were used. The *rbcL* gene is indicated by an arrow.

(B) RNA gel blot analysis of *petD* and *rbcL* RNA in wild-type (WT) and Zm-*bsf-1/-2* mutant plants. Total RNA (4 μg/lane) was analyzed by RNA gel blot hybridization using probes corresponding to *rbcL* and the second exon of *petD*, respectively. The *crp1* mutant (Barkan et al., 1994) was used as a control. The positions of RNA size markers are shown on the right. rRNAs were detected on the same filters by staining with methylene blue, as shown below.

maintaining *psbE* and *ndhE* stability and/or processing could not be excluded.

BSF, PrfB3, and CRP1 Cooperatively Affect Chloroplast Gene Expression

There are several reports of physical and functional interplay between two chloroplast RNA binding regulatory factors (Ostheimer et al., 2006; Schwarz et al., 2007; Asakura et al., 2008; Kroeger et al., 2009; Boulouis et al., 2011; Bentolila et al., 2012; Stoppel et al., 2012; Takenaka et al., 2012; Andrés-Colás et al., 2017; Guillaumot et al., 2017). Nevertheless, the significance of the cooperation between two chloroplast RNA binding proteins has rarely been addressed. Interestingly, our EMSA showed that PrfB3 increases the RNA binding ability of BSF. The combination of two different RNA binding proteins might establish new ribonucleoprotein architectures that efficiently increase their RNA binding affinities and facilitate the formation of ternary protein-RNA complexes (Hennig et al., 2014; Weidmann et al., 2016). However, in the presence of PrfB3, only the BSF-RNA complex levels increased, whereas no ternary protein-RNA complex was detected. Thus, it is likely that PrfB3 enhances the RNA binding ability of BSF independently of its association with RNAs. We suspect that in addition to direct binding to RNA, PrfB3 might bind to BSF

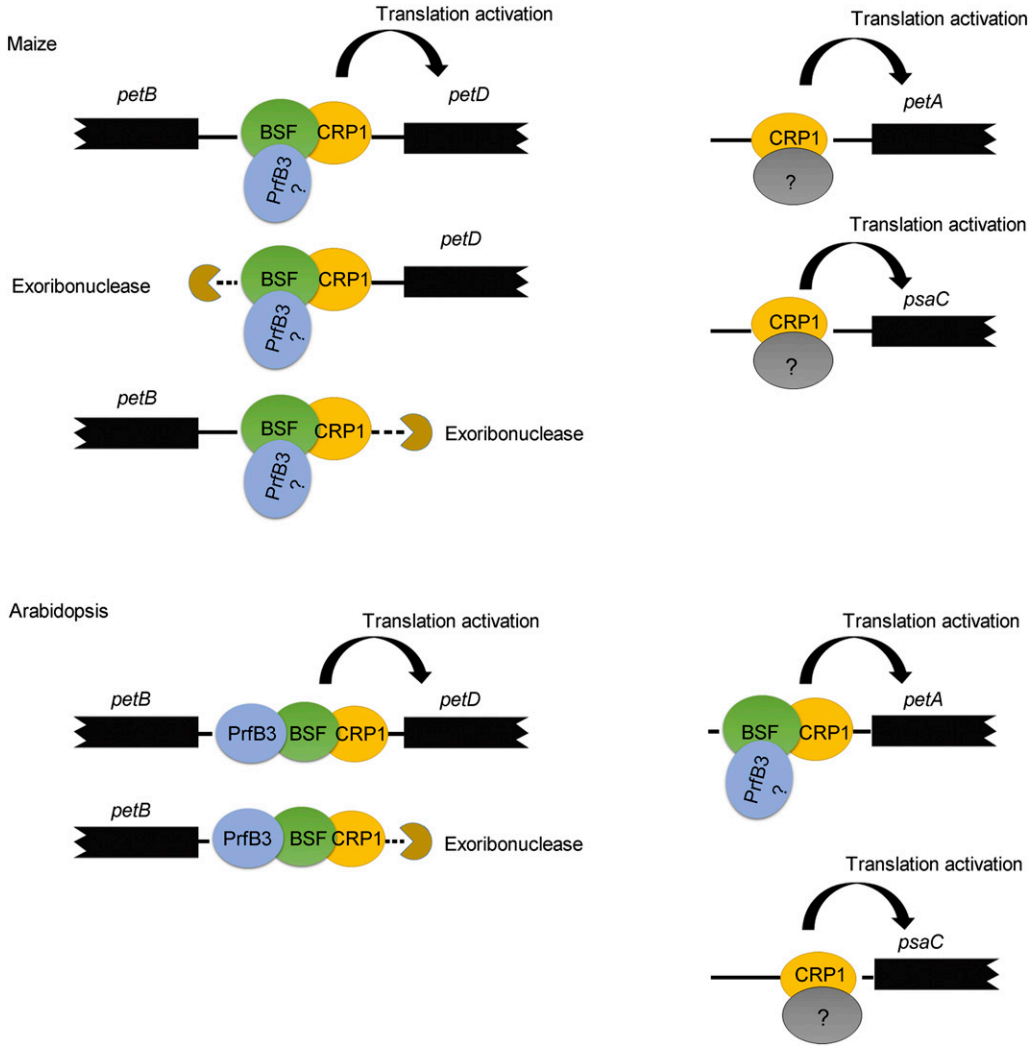

Figure 10. Model for the Cooperative Roles of CRP1, BSF, and PrfB3 in Maize and Arabidopsis.

The associations of the three factors with the RNAs that they regulate. Please note that the association of PrfB3 with the 5′ end of *petA* has not yet been demonstrated experimentally. The maize ortholog of PrfB3 was found in the rice but not the maize genome database (Stoppel et al., 2011). The function of BSF associated with the 3′ end of *petD* is still unclear and thus is not shown in this model. Arrows indicate an enhancement of translational efficiency. See "Discussion" for details.

and induce and/or stabilize its open conformation, thereby facilitating its association with RNA.

Despite the increased RNA binding ability of BSF in the presence of PrfB3, its RNA chaperone activity was not altered, suggesting that PrfB3 has no effect on the RNA chaperone activity of BSF. The relationship between RNA chaperone activity and RNA binding properties of RNA chaperone proteins remains unclear. Weakening the RNA binding ability of bacterial RNA chaperones CspA or CspE by mutating their RNA binding domains reduces their RNA chaperone activity (Phadtare et al., 2002a, 2002b). However, the opposite situation was observed for some other bacterial RNA chaperones, such as Suppressor of the td-phenotype A and Fertility inhibition O (Arthur et al., 2003; Mayer et al., 2007). Thus, the RNA chaperone activity and RNA binding properties appear to be relatively interdependent. Experimental data suggest that the protein domains crucial for chaperone activities are intrinsically disordered regions of RNA chaperones (Basu and Bahadur, 2016). It is likely that the association of PrfB3 with BSF activates only its RNA binding domain and not the intrinsically disordered region required for RNA melting.

Several studies have highlighted the important roles played by PPR-like proteins in chloroplast gene expression (Barkan and Small, 2014). How RNA binding proteins that bind single-stranded and especially long RNA segments access their binding sites in vivo, even when these binding sites are masked by secondary structures, remains largely unknown. Indeed, in vitro experiments showed that PPR10 binding is inhibited by even very weak RNA structures (McDermott et al., 2018), suggesting that RNA chaperones or RNA chaperone–like proteins might be required for minimizing the effects of such structures on PPR binding in vivo.

However, such factors that assist PPR protein binding have not yet been identified.

The RIP experiment together with in silico prediction of AtCRP1 binding sites indicated that AtCRP1 most likely binds directly to the 30- to 39-nucleotide segment upstream of the *petA* start codon (Ferrari et al., 2017). The predicted RNA secondary structure showed that this region can form a duplex with the BSF binding site. Considering the RNA chaperone activity of BSF, we hypothesize that BSF specifically binds to the RNA fragment next to the AtCRP1 binding site, which is able to pair with the AtCRP1 binding site, and unfolds the structured RNA to enable and/or facilitate binding of AtCRP1. Given that several stable secondary structures can form in the *petB-petD* intergenic region (Barkan et al., 1994), BSF might also assist in the binding of AtCRP1 and/or other translation activators via a similar mechanism, explaining the function of BSF in promoting *petD* translation. Nevertheless, we did not detect a defect in *psaC* translation in the *bsf* mutant (Figure 3), suggesting that the role of CRP1 in translational activation of *psaC* might not require the assistance of BSF.

Overall, our study indicates that the in vivo functions of PPR-like proteins, such as CRP1, indeed require the support of one or more RNA chaperone factors, although the presence of some PPR-like proteins alone is sufficient to block exoribonuclease activity or to remodel RNA structure in vitro (e.g., Prikryl et al., 2011; Hammani et al., 2012). PPR-like proteins might recruit distinct RNA chaperone(s) and form different RNA-protein complexes to regulate mRNA stability and/or translation depending on the distinct RNAs with which they associate. If this represents a general phenomenon, it suggests that the roles of PPR proteins and their (co)chaperones in regulating chloroplast gene expression have coevolved. Our immunoprecipitation-mass spectrometry data show that BSF also associates with other PPR proteins. It would be of great interest to investigate whether BSF supports the functions of these proteins by acting as an RNA chaperone–like factor.

Clarification of BSF Function in Arabidopsis and Maize

Bowman et al. (2013) suggested that RLSB (ZmBSF) is required for *rbcL* mRNA accumulation and translation in maize and Arabidopsis. By contrast, another study showed that BSF (referred to as PBR1) controls the expression of the chloroplast *ycf1* gene in Arabidopsis at the translational level (Yang et al., 2016). However, neither *rbcL* nor *ycf1* was identified as a BSF target in our genome-wide RIP and ribosome profiling assays. Therefore, our results argue against a direct role for BSF in the translation of *rbcL* and *ycf1* mRNA in maize and Arabidopsis, respectively. In contrast with Bowman et al. (2013), who investigated *rbcL* accumulation by RT-qPCR, our RNA gel blot analysis showed that *rbcL* mRNA levels were not altered in *zmbsf* mutants (Figure 9B), casting doubt on the role of BSF in *rbcL* stabilization. Interestingly, Yang et al. (2016) also found a defect in NDH complex accumulation in *bsf* mutants. We therefore propose a hypothesis explaining the NDH defect in *bsf*: The defects in *ndhD* translation (Figure 3) impair NDH complex biogenesis in *bsf*. However, the association of BSF with *ndhD* mRNA was not found in our RIP data (Figure 4). Similarly, ribosome profiling technology uncovered new targets that were missed in RIP assays for some PPR proteins (Rojas et al., 2018). It is likely that BSF does not bind directly to *ndhD* but binds indirectly through weak interaction with another protein. In that case, the association of BSF with *ndhD* might be prone to disruption during immunoprecipitation. Overall, our comprehensive assays of both maize and Arabidopsis mutants not only revealed the conserved function of this RNA chaperone–like protein between monocot and dicot plants, but they also clarified our understanding of its function.

Although the *psbB* transcription unit is highly conserved among land plants, there are still some differences in intergenic processing between monocot and dicot plants (Stoppel and Meurer, 2013). The most striking difference is *petB-petD* intergenic processing: The 3′ end of *petB* overlaps with the 5′ end of *petD* in maize but not in Arabidopsis (Stoppel et al., 2011). This overlapping region in maize is presumably bound by CRP1 to stabilize both the 5′ end of *petD* and the 3′ end of *petB*. Thus, the inactivation or inhibition of CRP1 activity would lead to the destabilization of monocistronic *petD* transcripts in maize (as shown in the schematic diagram in Figure 10). However, as discussed above, in Arabidopsis, BSF is associated with two sites of the *psbB* transcription unit (one in the *petB-petD* intergenic region and the other in the 3′ end of *petD*), which is quite different from the situation in maize (Figure 4). Although the function of BSF at the 3′ end of *petD* (if any) is unclear, it would be interesting to address whether the distinct actions of BSF are related to the differences in *petB-petD* intergenic processing between maize and Arabidopsis. In addition to this difference, our Ribo-seq assay also showed that BSF stimulates *petA* and *ndhD* translation but ZmBSF does not (Figure 10), suggesting that ZmBSF has lost these targets in monocots or that BSF has acquired new targets in vivo or during dicot evolution. The conserved and distinct roles of BSF in maize versus Arabidopsis suggest that BSF was recruited to promote mRNA stabilization and translation before the divergence of monocot and dicot plants but that it might have evolved differently in distinct species by losing or acquiring various RNA targets.

METHODS

Plant Materials and Growth Conditions

Arabidopsis (*Arabidopsis thaliana*) Columbia-0 (wild type) and T-DNA insertion lines *bsf-1* (*SALK_037487*), *bsf-2* (*SALK_072637*), and *prfB3* (*SALK_133921*) were obtained from the ABRC. Homozygous T-DNA insertions were identified by PCR using gene- and T-DNA-specific primers (all of the primers used in this study are listed in Supplemental Data Set 4). Maize (*Zea mays*) BSF is encoded by GRMZM2G087628 (B73 RefGen_v3) or Zm00001d044328 (B73 RefGen_v4). Evidence for orthology with Arabidopsis BSF can be found at http://cas-pogs.uoregon.edu/#/pog/10688. The *zmbsf1-1* and *zmbsf1-2* mutant alleles were described previously and were referred to as *rlsb-1* and *rlsb-2*, respectively (Bowman et al., 2013). Heteroallelic progeny of a complementation test cross between plants heterozygous for each of these alleles was used for all experiments.

Maize seeds were sown in soil, and the plants were grown under a diurnal cycle (16 h light/8 h dark) at 28°C and 26°C for the light and dark periods, respectively. The plants were illuminated with a light intensity of $\sim$300 μmol m^{-2} s^{-1} [16 cool white, high output fluorescent lamps (F72T12/CS/VHO, Sylvania) in combination with 12 100-watt soft white incandescent bulbs (Sylvania)]. The second and third leaves were harvested 8 or 9 d after planting and frozen in liquid nitrogen before processing for Ribo-seq or RNA extraction. Arabidopsis seeds were sterilized by

incubation in a solution of 1% (w/v) bleach and 0.1% (w/v) SDS for 10 min, followed by washing with 70% (v/v) ethanol and three washes with sterile water. The seeds were sown on sterile MS medium (4.33 g/L MS Basal Medium [Sigma-Aldrich], 2% [w/v] Suc, and 0.3% [w/v] Phytagel [Sigma-Aldrich], pH 5.7). The plants were grown in a growth chamber at 22°C under a diurnal cycle (12 h light/12 h dark) at a light intensity of 100 μmol m^{-2} s^{-1} (eight 28-watt fluorescent lamps [TLS 28W/865, Philips]).

Complementation of the *bsf* Mutant

The coding sequence of *BSF* was cloned into the *Bam*HI and *Kpn*I sites of the binary vector pSN1301 (Zhou et al., 2009), in which it was constitutively expressed under the control of the cauliflower mosaic virus 35S promoter. This construct was then transferred into *Agrobacterium tumefaciens* strain C58 and introduced into *bsf-1* by the floral dip method (Clough and Bent, 1998). The transformants were selected on MS medium containing 50 μg mL^{-1} hygromycin B.

Chlorophyll Fluorescence Measurements

Chlorophyll fluorescence measurements were performed using a CF Imager (Technologica) according to the manufacturer's instructions. Before each measurement, the leaves were dark-adapted for 10 min. The minimum fluorescence yield (F_0) and the maximum fluorescence yield (F_m) were measured. The maximal photochemical efficiency of PSII was calculated based on the F_v to F_m ratio [$F_v/F_m = (F_m - F_0)/F_m$]. Image data acquired in each experiment were normalized to a false color scale, with arbitrarily assigned extreme values of 0.01 (lowest) and 0.85 (highest). Thus, the highest and lowest F_v/F_m values are represented by the red and blue extremes of the color scale, respectively.

RNA Preparation and RNA Gel Blotting

Frozen leaves from 14-d-old plants were ground in liquid nitrogen and subjected to RNA extraction using an RNeasy Plant Mini kit (Qiagen). For RNA gel blotting, the RNA samples were electrophoretically separated in formaldehyde-containing 1.2% (w/v) agarose gels and transferred onto Hybond N^+ membranes by capillary blotting. Hybridization probes of chloroplast genes were generated by PCR amplification using gene-specific primers and purified by agarose gel electrophoresis, followed by extraction from an excised gel slice. The hybridization probes were labeled with [α^{32}P]-deoxycytidine triphosphate or biotin using the random priming method (>200 bp) or 3′ end labeling (<200 bp). RNA gel blot hybridization of the maize mutant was performed as described previously (Barkan, 1998) using a radiolabeled PCR product mapping to *petD* exon 2 (coordinates 75547–75895 in the maize chloroplast genome, accession number NC_001666).

Primer Extension and RNase Protection Assays

Primer extension assays were conducted as described before (Barkan, 2011b), except that dideoxyribonucleoside triphosphates were omitted from the reactions. Extension reactions were performed at 50°C. The products were separated on a denaturing 15% polyacrylamide gel in 1× Tris-Borate-EDTA (TBE) buffer.

RNase protection assays were performed using an RPA III kit (Ambion) according to the manufacturer's instructions. Briefly, the probes were transcribed and radiolabeled in vitro using the annealed primer pairs. The probes were gel purified and hybridized to 10 μg total RNA in hybridization buffer at 42°C. An RNase A/RNase T1 mixture was added to the hybridization buffer to a final dilution of 1:100. The reaction mixtures were incubated for 30 min at 37°C. Nucleic acids were ethanol precipitated and electrophoresed on a denaturing 15% polyacrylamide gel in 1× TBE buffer.

RT-PCR and DNA Sequencing

RNA samples were treated with DNase I for 30 min at 37°C and transcribed using SuperScript III reverse transcriptase (Invitrogen) with random primers. The cDNAs were used as templates for PCR with gene-specific primers, which are listed in Supplemental Data Set 4. PCR was performed in a T100 Thermal Cycler (Bio-Rad) using PrimeSTAR GXL Premix (Takara) according to the manufacturer's instructions. For DNA sequencing, the amplification products were separated by electrophoresis in 1.0% (w/v) agarose gels and purified for sequencing (Beijing Genomics Institute). The sequencing data were analyzed using Chrosome software.

Protein Expression and Antibody Production

To produce recombinant MBP-BSF proteins, the coding sequence of BSF lacking the transit peptide sequence (amino acids 1–63) was PCR amplified and inserted into the *Bam*HI and *Sal*I sites of the pETMALc-H vector. The fusion protein was expressed in BL21 (Rosetta2) *Escherichia coli* cells by inducing log phase cultures with 0.5 mM Isopropyl β-D-Thiogalactoside at 17°C for 18 h. Purification on amylose beads and TEV protease cleavage were performed as described (Chi et al., 2012). Gel filtration chromatography of the cleavage products was performed on a HiLoad™16/600 Superdex200 pg column (GE Healthcare) according to the manufacturer's instructions. Recombinant PrfB3 protein was generated as described before (Stoppel et al., 2011).

To produce antibodies against BSF, the recombinant protein was injected into rabbits five times at 1-week intervals, and the antiserum obtained was affinity purified before immunoblotting.

Protein Isolation and Analysis

Stromal, envelope, and thylakoid membrane proteins were isolated as described (Williams and Barkan, 2003). The stromal fractions were prepared as described (Chi et al., 2012). For total protein isolation, 0.1 g of Arabidopsis leaf tissue was homogenized in isolation medium (125 mM Tris, 1% [w/v] SDS, 10% glycerol [v/v], and 50 mM $Na_2S_2O_5$). The homogenate was filtered through two layers of Miracloth and centrifuged at 15,000*g* for 10 min. The soluble and membrane proteins were separated by 10% and 15% (w/v) SDS-PAGE and transferred onto nitrocellulose membranes. Immunoblot detection was performed with antibodies of for BSF and PrfB3 at 1:2,000 dilution, FLAG (MBL, #M185-3L) and ACTIN (Sigma-Aldrich, #A0480) at 1:5,000 dilution, and GST (Sigma-Aldrich, # G7781) and His (Sigma-Aldrich, # SAB1305538) at 1:1,000 dilution using an enhanced chemiluminescence system. Antibodies used for detection of thylakoid membrane complex subunits were described previously (Zhang et al., 1999).

GFP Assay

Plasmids expressing GFP fusion proteins were constructed as described (Chi et al., 2012). The proteins were transiently expressed in protoplasts prepared from Arabidopsis leaves (Kovtun et al., 2000), and fluorescence was visualized 12 h after transformation. Fluorescence analysis was performed using an LSM 510 META confocal laser scanning system (Zeiss).

RNA Coimmunoprecipitation and Slot-Blot Hybridization

Chloroplasts and stromal extract were prepared from 2-week-old Arabidopsis plants as described (Stoppel et al., 2011; Paieri et al., 2018). Each 500-μg stromal extract sample was diluted with the same volume of Coimmunoprecipitation buffer (20 mM Tris [pH 7.5], 150 mM NaCl, 1 mM EDTA, 0.5% [v/v] Nonidet P40, and Protease Inhibitor Cocktail [Roche]) and incubated with anti-BSF serum (10 μL) or preimmune serum (10 μL) for 1 h at

4°C with rotation (8 rpm). After the addition of 50 μL SiMAG-Protein G beads (Chemicell), the sample was incubated for 1 h at 4°C with rotation (8 rpm). Following three washes with Coimmunoprecipitation buffer, RNA was extracted from the sample with TRIzol reagent (Invitrogen), precipitated with ethanol, and used for deep sequencing or slot-blot hybridization.

For RNA deep sequencing, libraries were prepared using a ScriptSeq v2 RNA-seq Library Preparation Kit (Epicentre) according to the manufacturer's instructions. Sequencing (2 × 150 bp, v2 chemistry) was performed on a MiSeq sequencer (Illumina), yielding 17.4 Mio primary reads for anti-BSF serum and 25.6 Mio reads for the preimmune serum control. Paired trimmed reads were aligned to the Arabidopsis chloroplast genome (accession number NC_000932.1) using the CLC Genomics Workbench 6.5.1 (Qiagen) with the following parameters: mismatch cost = 2, insertion cost = 3, deletion cost = 3, length fraction = 0.5, similarity fraction = 0.8, global alignment = no; autodetect paired distances = yes. Coverage data (reads/nucleotides) were extracted and analyzed with Excel. The second replicate yielded 17.2 Mio reads for anti-BSF serum and 13.6 Mio reads for the preimmune serum control.

To generate the graph shown in Figure 4A, reads of the two replicates aligned in CLC Genomics Workbench were extracted as Binary Alignment Map (BAM) files and sorted with Galaxy using the SortSam tool (version 2.7.1.1). With use of the bamCoverage tool (version 3.0.2), the sorted BAM files were converted into RPKM-normalized bigwig files and displayed in Integrative Genome Browser. The differential enrichment of BSF/control values of the two replicates was displayed across the entire chloroplast genome.

Slot-blot experiments were performed as described before (Manavski et al., 2015). Three slot blot membranes were prepared; multiple reprobing was performed after stripping off the previous probes.

EMSAs

Biotin-labeled RNAs were synthesized by Takara Company. The labeled RNA (1 nM) was incubated with increasing amounts of protein (as indicated) in a buffer containing 100 mM HEPES, pH 7.3; 200 mM KCl; 10 mM $MgCl_2$; and 10 mM DTT at 25°C for 30 min. As competitors, unlabeled poly(A), poly (U), poly(G), and poly(C) were used in 10×, 100×, and 500× molar excess over the labeled *petB* 3′ UTR probes. The samples were separated on a nondenaturing 6% PAGE (w/v) gel prepared in 0.5× TBE buffer.

Protein Pull-Down and Coimmunoprecipitation Assays

The GST-BSF fusion protein and PrfB3-maltose binding protein (MBP) fusion protein were purified using glutathione beads (GE Healthcare), and amylose resin (New England Biolabs), respectively, according to the manufacturer's protocol. A 2-μg sample of BSF-GST-bound glutathione beads was incubated with 2 μg of MBP-PrfB3, MBP-AtCRP1, MBP-ECD1, or MBP alone in binding buffer containing 20 mM Tris-HCl, pH 7.5, and 200 mM NaCl at 4°C for 2 h. The beads were washed three times with washing buffer (20 mM Tris-HCl, pH 7.5, and 200 mM NaCl). The protein was eluted from the beads by boiling in 50 μL of 2× sampling buffer, loaded onto a 15% SDS-PAGE gel, and analyzed by immunoblot analysis using anti-BSF antibody.

For the coimmunoprecipitation assays, 0.1 g of leaf tissue from 2-week-old Arabidopsis seedlings was homogenized in PBS buffer containing 1% (w/v) dodecyl-β-D-maltopyranoside. The extracts were centrifuged at 12,000*g* for 15 min at 4°C and the supernatant was collected. Total protein with or without RNase treatment (treated with RNase I at 37°C for 30 min) was incubated with the preserum (Pre) and antibodies against ECD1 and PrfB3 coupled covalently to protein A Sepharose beads overnight at 4°C, respectively. After the beads were washed five times with PBS containing 0.5% Nonidet P40, the bound proteins were eluted with 0.1 M Gly (pH 3.0), separated by SDS-PAGE, and analyzed by immunoblotting with BSF antibodies. As a control, the supernatants obtained from coimmunoprecipitation were also tested by immunoblotting with BSF antibodies.

Mass Spectrometry Analysis

To purify BSF-associated proteins for mass spectrometry analysis, the DNA encoding two copies of FLAG and the immunoglobulin binding domain of protein A from *Staphylococcus aureus* (IgG) (Rubio et al., 2005) was synthesized and cloned into the *Sac*I and *Kpn*I sites of pUC18 plasmid (Thermo Fisher Scientific, #SD0051). Then the coding sequences of *BSF* were cloned into *Bam*HI and *Kpn*I sites of this construct to generate a *BSF-FLAG-IgG* fused gene. . This *BSF-FLAG-IgG* fused gene was excised from this construct by digestion with *Sac*I and *Bam*HI, cloned into pSN1301 vector, and transformed into wild-type Arabidopsis by the floral dip method (Clough and Bent, 1998). Similarly, a transgenic line expressing FLAG-IgG-tagged FtsHi1 was constructed as a negative control. Immunoprecipitation of total proteins from these transgenic lines was performed using ANTI-FLAG M2 magnetic beads (Sigma-Aldrich) according to the manufacturer's instructions. Proteins were eluted from the beads by competition with FLAG peptide and were then resolved by SDS-PAGE. Protein bands were excised from the SDS-PAGE gel and digested in-gel as described by Shevchenko et al. (2006). Tryptic peptides were analyzed using an LTQ Orbitrap Elite mass spectrometer (Thermo Fisher Scientific) coupled online to an Easy-nLC 1000 (Thermo Fisher Scientific) in data-dependent mode. Data were analyzed using a prerelease version of Thermo Scientific Proteome Discoverer software version 1.4.

Overlay Assay

For the protein overlay assay, total proteins from the wild type and *bsf* mutant were separated by SDS-PAGE and transferred onto nitrocellulose membranes. The membranes were blocked with 5% skim milk overnight and incubated with 0.25 mg/mL recombinant MBP-HIS-AtCRP1, MBP-HIS-ECD1, or MBP protein for 2 h. After incubation, the membranes were washed three times with Tween/Tris-Buffered Salt solution buffer and probed with anti-His and anti-BSF antibodies.

BN-PAGE

BN-PAGE was performed as described by Peng et al. (2006) with minor modifications. Chloroplast stroma from transgenic plants expressing FLAG-IgG-tagged AtCRP1 was solubilized with 1% (v/v) β-dodecyl-maltoside and subjected to 4.5 to 13.5% (w/v) BN-PAGE. For two-dimensional analysis, excised BN-PAGE lanes were soaked in SDS sample buffer containing 2.5% (v/v) β-mercaptoethanol for 30 min and layered onto 1-mm-thick 10% (w/v) SDS-polyacrylamide gels. After electrophoresis, the proteins were stained and transferred to nitrocellulose membranes for immunoblot analysis.

Yeast Two-Hybrid Assay

Yeast two-hybrid assays were performed using the Matchmaker Gold system (Clontech). The pGADT7 and pGBKT7 plasmids were used to construct the prey and bait plasmids, respectively. The prey and bait plasmids were cotransformed into yeast strain Y2HGold and plated onto SD/-Leu-Trp-His dropout plates containing X-α-Gal to allow a blue color to develop. Yeast cells cotransformed with pGBKT7-53 and pGADT7-T were used as a positive control, and yeast cells transformed with pGBKT7-Lam and pGADT7-T were used as a negative controls.

BiFC Assay

BiFC assays were performed essentially as described by Walter et al. (2004). Fragments encoding full-length BSF and MORF9 were amplified by PCR from wild-type cDNA and ligated into pSAT4A-cEYFP-N1 to produce BSF-cYFP and MORF9-cYFP, respectively. The coding regions of *AtCRP1* and *ECD1* were amplified by PCR and ligated into pSAT4A-nEYFP-N1 after digestion to produce AtCRP1-nYFP and ECD1-nYFP, respectively. Combinations of the indicated plasmids were cotransformed into Arabidopsis protoplasts via PEG-calcium-mediated transformation (Kovtun et al., 2000). YFP fluorescence was visualized 12 to 18 h after transformation under a confocal laser-scanning microscope (LSM 510 Meta; Zeiss).

RNA Chaperone Assay

DNA-melting activity was measured as described previously (Phadtare et al., 2002a). The beacon used in this study was an 82-nt hairpin-shaped molecule labeled with a fluorophore and quencher: tetramethyl rhodamine-AGGGTTCTTTGTGGTGTTTTTATCTGTGCTTCCCTATGCACCGCCGAC-GACAGTCGCTAACCTCTCGCTAAGAACCCT-DABCYL; the molecular beacon was synthesized by Takara Company. Fluorescence measurements were performed using an F7000 spectrofluorometer (Hitachi). The excitation and emission wavelengths used were 555 and 575 nm, respectively. The fluorescence of a 100-μL solution of 32 nM molecular beacon dissolved in 20 mM Tris-HCl, pH 7.5, containing 1 mM $MgCl_2$ was monitored when proteins shown in Figure 8C were added. The reactions were conducted at room temperature.

The complementation of *E. coli* BX04 mutant cells was performed as described (Phadtare et al., 2002a). The cDNA encoding mature BSF protein was introduced into pINIII and transformed into *E. coli* BX04 cells. As a positive control, the pNIII plasmid containing *cspA* was also constructed. *E. coli* strain BX04 cells were grown in Luria-Bertani (LB) medium, and a serially diluted culture was spotted onto LB plates and incubated at 37°C or 20°C.

DMS Probing

DMS probing was performed as recently described by Meurer et al. (2017).

Ribosome Profiling

Ribosome footprint preparation, library construction, and data analyses were performed as described previously (Chotewutmontri and Barkan, 2018). Maize Ribo-seq was performed using the apical halves of the second and third leaves that emerged in 9-d-old plants, pooling tissue from two mutant seedlings and two phenotypically normal siblings. Ribosome profiling of the Arabidopsis *bsf* mutants was performed using the aerial portions of 20-d-old seedlings, using pools of three mutant seedlings and three siblings with normal phenotypes. Raw and normalized read counts mapped to each chloroplast gene are provided in Supplemental Data Set 5.

Accession Numbers

Sequence data from this article can be found in the GenBank/EMBL library under the following accession numbers: BSF (AT1G71720), PrfB3 (AT3G57190), and AtCRP1 (AT5G42310). The mass spectrometry proteomics data have been deposited in the ProteomeXchange Consortium via the PRoteomics IDEntifications (PRIDE; Perez-Riverol et al., 2019) partner repository under dataset identifier PXD013325. All sequencing reads of the ribosome profiling assay have been deposited in the Sequence Read Archive under accession number PRJNA530618. The sequencing data for the RIP-seq assays can be found in the Gene Expression Omnibus under accession number GSE 129411.

Supplemental Data

Supplemental Figure 1. Expression of BSF in wild-type and *bsf* plants.

Supplemental Figure 2. Phenotypes of BSF-complemented plants.

Supplemental Figure 3. RNA gel blot analysis of chloroplast mRNAs associated with BSF in *bsf* and *prfB3* plants.

Supplemental Figure 4. Accumulation of monocistronic *petD* mRNA in *bsf* and *prfB3* plants.

Supplemental Figure 5. Ribonuclease protection mapping of processed and spliced sites of the *psbB-psbT-psbH-petB-petD* transcription unit.

Supplemental Figure 6. Subcellular localization and expression analysis of BSF protein.

Supplemental Figure 7. differential enrichment (BSF/control) of the *petA*, *petB*, and *petD* loci.

Supplemental Figure 8. RNase i treatment of stroma effectively degrades RNA.

Supplemental Figure 9. Identification of transgenic lines expressing FLAG-IgG-Tagged AtCRP1 or BSF by immunoblot assays.

Supplemental Figure 10. BSF-AtCRP1-PrfB3 complex revealed by 2D BN-PAGE assay.

Supplemental Figure 11. PrfB3 immunopurified from a transgenic line expressing BSF-FLAG-IgG.

Supplemental Figure 12. RNA binding ability of BSF in the presence of RNA competitors.

Supplemental Figure 13. The *petB/D* binding site of PrfB3.

Supplemental Figure 14. EMSA with BSF in combination of MBP.

Supplemental Figure 15. Chaperone activity of BSF in combination with PrfB3.

Supplemental Table. Identification of chloroplast-localized proteins associated with BSF by mass spectrometry.

Supplemental Data Set 1. Reads/nucleotides generated by RIP using BSF serum and preimmune serum from replicate one.

Supplemental Data Set 2. Peptides of BSF-associated proteins identified by mass spectrometry.

Supplemental Data Set 3. Fluorescent signals from the 82-nt molecular beacon labeled with a fluorophore and quencher and incubated with BSF.

Supplemental Data Set 4. Primers used in this study.

Supplemental Data Set 5. Raw and normalized read counts mapped to each chloroplast gene used for ribosome profiling.

ACKNOWLEDGMENTS

We would like to thank Jean-David Rochaix from University of Geneva and Chuanxiao Xie from the Institute of Crops, CAAS for critical comments on this work. We are also grateful to Linsheng Song from Dalian Ocean University for kindly providing the pINIII plasmid. This work was supported by the Chinese Academy of Sciences (CAS) Strategic Priority Research Program (XDB17030100), the Ministry of Science and Technology of the People's Republic of China (Chinese Ministry of Science and Technology) Major State Basic Research Development Program (2015CB150101), the

German Science Foundation (DFG; TRR175 A03 to J.M.), and the US National Science Foundation (IOS-1339130 to A.B.).

AUTHOR CONTRIBUTIONS

J.J., X.C., N.M., R.W.-C., B.H., A. Brachmann, D.J., M.O., Y.L., and W.C. performed the experiments; A. Barkan, J.M., L.Z., and W.C. analyzed the data; N.M., A. Barkan, J.M., and L.Z. revised the article; W.C. conceived this study and wrote the article.

Received December 14, 2018; revised March 19, 2019; accepted April 7, 2019; published April 8, 2019.

REFERENCES

Andrés-Colás, N., Zhu, Q., Takenaka, M., De Rybel, B., Weijers, D., and Van Der Straeten, D. (2017). Multiple PPR protein interactions are involved in the RNA editing system in *Arabidopsis* mitochondria and plastids. Proc. Natl. Acad. Sci. USA **114:** 8883–8888.

Arthur, D.C., Ghetu, A.F., Gubbins, M.J., Edwards, R.A., Frost, L.S., and Glover, J.N. (2003). FinO is an RNA chaperone that facilitates sense-antisense RNA interactions. EMBO J. **22:** 6346–6355.

Asakura, Y., and Barkan, A. (2006). *Arabidopsis* orthologs of maize chloroplast splicing factors promote splicing of orthologous and species-specific group II introns. Plant Physiol. **142:** 1656–1663.

Asakura, Y., Bayraktar, O.A., and Barkan, A. (2008). Two CRM protein subfamilies cooperate in the splicing of group IIB introns in chloroplasts. RNA **14:** 2319–2332.

Barkan, A. (1988). Proteins encoded by a complex chloroplast transcription unit are each translated from both monocistronic and polycistronic mRNAs. EMBO J. **7:** 2637–2644.

Barkan, A. (1998). Approaches to investigating nuclear genes that function in chloroplast biogenesis in land plants. Methods Enzymol. **297:** 38–57.

Barkan, A. (2011a). Expression of plastid genes: Organelle-specific elaborations on a prokaryotic scaffold. Plant Physiol. **155:** 1520–1532.

Barkan, A. (2011b). Studying the structure and processing of chloroplast transcripts. Methods Mol. Biol. **774:** 183–197.

Barkan, A., and Goldschmidt-Clermont, M. (2000). Participation of nuclear genes in chloroplast gene expression. Biochimie **82:** 559–572.

Barkan, A., and Small, I. (2014). Pentatricopeptide repeat proteins in plants. Annu. Rev. Plant Biol. **65:** 415–442.

Barkan, A., Walker, M., Nolasco, M., and Johnson, D. (1994). A nuclear mutation in maize blocks the processing and translation of several chloroplast mRNAs and provides evidence for the differential translation of alternative mRNA forms. EMBO J. **13:** 3170–3181.

Basu, S., and Bahadur, R.P. (2016). A structural perspective of RNA recognition by intrinsically disordered proteins. Cell. Mol. Life Sci. **73:** 4075–4084.

Bentolila, S., Heller, W.P., Sun, T., Babina, A.M., Friso, G., van Wijk, K.J., and Hanson, M.R. (2012). RIP1, a member of an *Arabidopsis* protein family, interacts with the protein RARE1 and broadly affects RNA editing. Proc. Natl. Acad. Sci. USA **109:** E1453–E1461.

Bokinsky, G., Nivón, L.G., Liu, S., Chai, G., Hong, M., Weeks, K.M., and Zhuang, X. (2006). Two distinct binding modes of a protein cofactor with its target RNA. J. Mol. Biol. **361:** 771–784.

Boulouis, A., Raynaud, C., Bujaldon, S., Aznar, A., Wollman, F.A., and Choquet, Y. (2011). The nucleus-encoded *trans*-acting factor MCA1 plays a critical role in the regulation of cytochrome *f* synthesis in *Chlamydomonas* chloroplasts. Plant Cell **23:** 333–349.

Bowman, S.M., Patel, M., Yerramsetty, P., Mure, C.M., Zielinski, A.M., Bruenn, J.A., and Berry, J.O. (2013). A novel RNA binding protein affects rbcL gene expression and is specific to bundle sheath chloroplasts in C4 plants. BMC Plant Biol. **13:** 138.

Bycroft, M., Hubbard, T.J., Proctor, M., Freund, S.M., and Murzin, A.G. (1997). The solution structure of the S1 RNA binding domain: A member of an ancient nucleic acid-binding fold. Cell **88:** 235–242.

Chi, W., Ma, J., Zhang, D., Guo, J., Chen, F., Lu, C., and Zhang, L. (2008). The pentratricopeptide repeat protein DELAYED GREENING1 is involved in the regulation of early chloroplast development and chloroplast gene expression in *Arabidopsis.* Plant Physiol. **147:** 573–584.

Chi, W., He, B., Mao, J., Li, Q., Ma, J., Ji, D., Zou, M., and Zhang, L. (2012). The function of RH22, a DEAD RNA helicase, in the biogenesis of the 50S ribosomal subunits of *Arabidopsis* chloroplasts. Plant Physiol. **158:** 693–707.

Chi, W., He, B., Manavski, N., Mao, J., Ji, D., Lu, C., Rochaix, J.D., Meurer, J., and Zhang, L. (2014). RHON1 mediates a Rho-like activity for transcription termination in plastids of *Arabidopsis thaliana.* Plant Cell **26:** 4918–4932.

Chotewutmontri, P., and Barkan, A. (2018). Multilevel effects of light on ribosome dynamics in chloroplasts program genome-wide and *psbA*-specific changes in translation. PLoS Genet. **14:** e1007555.

Clough, S.J., and Bent, A.F. (1998). Floral dip: A simplified method for Agrobacterium-mediated transformation of Arabidopsis thaliana. Plant J. **16:** 735–743.

Company, M., Arenas, J., and Abelson, J. (1991). Requirement of the RNA helicase-like protein PRP22 for release of messenger RNA from spliceosomes. Nature **349:** 487–493.

Doetsch, M., Schroeder, R., and Fürtig, B. (2011). Transient RNA-protein interactions in RNA folding. FEBS J. **278:** 1634–1642.

Duval, M., Korepanov, A., Fuchsbauer, O., Fechter, P., Haller, A., Fabbretti, A., Choulier, L., Micura, R., Klaholz, B.P., Romby, P., Springer, M., and Marzi, S. (2013). *Escherichia coli* ribosomal protein S1 unfolds structured mRNAs onto the ribosome for active translation initiation. PLoS Biol. **11:** e1001731.

Ferrari, R., Tadini, L., Moratti, F., Lehniger, M.K., Costa, A., Rossi, F., Colombo, M., Masiero, S., Schmitz-Linneweber, C., and Pesaresi, P. (2017). CRP1 Protein: (dis)similarities between *Arabidopsis thaliana* and *Zea mays.* Front. Plant Sci. **8:** 163.

Fisk, D.G., Walker, M.B., and Barkan, A. (1999). Molecular cloning of the maize gene crp1 reveals similarity between regulators of mitochondrial and chloroplast gene expression. EMBO J. **18:** 2621–2630.

Germain, A., Hotto, A.M., Barkan, A., and Stern, D.B. (2013). RNA processing and decay in plastids. Wiley Interdiscip. Rev. RNA **4:** 295–316.

Gribskov, M. (1992). Translational initiation factors IF-1 and eIF-2 alpha share an RNA-binding motif with prokaryotic ribosomal protein S1 and polynucleotide phosphorylase. Gene **119:** 107–111.

Guillaumot, D., Lopez-Obando, M., Baudry, K., Avon, A., Rigaill, G., Falcon de Longevialle, A., Broche, B., Takenaka, M., Berthomé, R., De Jaeger, G., Delannoy, E., and Lurin, C. (2017). Two interacting PPR proteins are major *Arabidopsis* editing factors in plastid and mitochondria. Proc. Natl. Acad. Sci. USA **114:** 8877–8882.

Hammani, K., Cook, W.B., and Barkan, A. (2012). RNA binding and RNA remodeling activities of the half-a-tetratricopeptide (HAT) protein HCF107 underlie its effects on gene expression. Proc. Natl. Acad. Sci. USA **109:** 5651–5656.

Hammani, K., Bonnard, G., Bouchoucha, A., Gobert, A., Pinker, F., Salinas, T., and Giegé, P. (2014). Helical repeats modular proteins are major players for organelle gene expression. Biochimie **100:** 141–150.

Hennig, J., Militti, C., Popowicz, G.M., Wang, I., Sonntag, M., Geerlof, A., Gabel, F., Gebauer, F., and Sattler, M. (2014). Structural basis for the assembly of the Sxl-Unr translation regulatory complex. Nature **515:** 287–290.

Herschlag, D. (1995). RNA chaperones and the RNA folding problem. J. Biol. Chem. **270:** 20871–20874.

Huang, M., Friso, G., Nishimura, K., Qu, X., Olinares, P.D., Majeran, W., Sun, Q., and van Wijk, K.J. (2013). Construction of plastid reference proteomes for maize and *Arabidopsis* and evaluation of their orthologous relationships: The concept of orthoproteomics. J. Proteome Res. **12:** 491–504.

Ingolia, N.T. (2016). Ribosome footprint profiling of translation throughout the genome. Cell **165:** 22–33.

Jenkins, B.D., and Barkan, A. (2001). Recruitment of a peptidyl-tRNA hydrolase as a facilitator of group II intron splicing in chloroplasts. EMBO J. **20:** 872–879.

Jiang, T., Zhang, J., Rong, L., Feng, Y., Wang, Q., Song, Q., Zhang, L., and Ouyang, M. (2018). ECD1 functions as an RNA-editing *trans*-factor of *rps14*-149 in plastids and is required for early chloroplast development in seedlings. J. Exp. Bot. **69:** 3037–3051.

Jiang, W., Hou, Y., and Inouye, M. (1997). CspA, the major cold-shock protein of *Escherichia coli*, is an RNA chaperone. J. Biol. Chem. **272:** 196–202.

Kang, H., Park, S.J., and Kwak, K.J. (2013). Plant RNA chaperones in stress response. Trends Plant Sci. **18:** 100–106.

Kikuchi, S., et al. (2018). A Ycf2-FtsHi heteromeric AAA-ATPase complex is required for chloroplast protein import. Plant Cell **30:** 2677–2703.

Kovtun, Y., Chiu, W.L., Tena, G., and Sheen, J. (2000). Functional analysis of oxidative stress-activated mitogen-activated protein kinase cascade in plants. Proc. Natl. Acad. Sci. USA **97:** 2940–2945.

Kroeger, T.S., Watkins, K.P., Friso, G., van Wijk, K.J., and Barkan, A. (2009). A plant-specific RNA-binding domain revealed through analysis of chloroplast group II intron splicing. Proc. Natl. Acad. Sci. USA **106:** 4537–4542.

Langer, D., Lottspeich, F., and Zillig, W. (1994). A subunit of an archaeal DNA-dependent RNA polymerase contains the S1 motif. Nucleic Acids Res. **22:** 694.

Lempereur, L., Nicoloso, M., Riehl, N., Ehresmann, C., Ehresmann, B., and Bachellerie, J.P. (1985). Conformation of yeast 18S rRNA. Direct chemical probing of the 5′ domain in ribosomal subunits and in deproteinized RNA by reverse transcriptase mapping of dimethyl sulfate-accessible. Nucleic Acids Res. **13:** 8339–8357.

Manavski, N., Torabi, S., Lezhneva, L., Arif, M.A., Frank, W., and Meurer, J. (2015). HIGH CHLOROPHYLL FLUORESCENCE145 binds to and stabilizes the *psaA* 5′ UTR *via* a newly defined repeat motif in embryophyta. Plant Cell **27:** 2600–2615.

Manavski, N., Schmid, L.M., and Meurer, J. (2018). RNA-stabilization factors in chloroplasts of vascular plants. Essays Biochem. **62:** 51–64.

Martin, W., Stoebe, B., Goremykin, V., Hapsmann, S., Hasegawa, M., and Kowallik, K.V. (1998). Gene transfer to the nucleus and the evolution of chloroplasts. Nature **393:** 162–165.

Mayer, O., Rajkowitsch, L., Lorenz, C., Konrat, R., and Schroeder, R. (2007). RNA chaperone activity and RNA-binding properties of the *E. coli* protein StpA. Nucleic Acids Res. **35:** 1257–1269.

McDermott, J.J., Civic, B., and Barkan, A. (2018). Effects of RNA structure and salt concentration on the affinity and kinetics of interactions between pentatricopeptide repeat proteins and their RNA ligands. PLoS One **13:** e0209713.

Meierhoff, K., Felder, S., Nakamura, T., Bechtold, N., and Schuster, G. (2003). HCF152, an *Arabidopsis* RNA binding pentatricopeptide repeat protein involved in the processing of chloroplast *psbB-psbT-psbH-petB-petD* RNAs. Plant Cell **15:** 1480–1495.

Meurer, J., Meierhoff, K., and Westhoff, P. (1996). Isolation of high-chlorophyll-fluorescence mutants of *Arabidopsis thaliana* and their characterisation by spectroscopy, immunoblotting and northern hybridisation. Planta **198:** 385–396.

Meurer, J., Lezhneva, L., Amann, K., Gödel, M., Bezhani, S., Sherameti, I., and Oelmüller, R. (2002). A peptide chain release factor 2 affects the stability of UGA-containing transcripts in *Arabidopsis* chloroplasts. Plant Cell **14:** 3255–3269.

Meurer, J., Schmid, L.M., Stoppel, R., Leister, D., Brachmann, A., and Manavski, N. (2017). PALE CRESS binds to plastid RNAs and facilitates the biogenesis of the 50S ribosomal subunit. Plant J. **92:** 400–413.

Ostheimer, G.J., Williams-Carrier, R., Belcher, S., Osborne, E., Gierke, J., and Barkan, A. (2003). Group II intron splicing factors derived by diversification of an ancient RNA-binding domain. EMBO J. **22:** 3919–3929.

Ostheimer, G.J., Rojas, M., Hadjivassiliou, H., and Barkan, A. (2006). Formation of the CRS2-CAF2 group II intron splicing complex is mediated by a 22-amino acid motif in the COOH-terminal region of CAF2. J. Biol. Chem. **281:** 4732–4738.

Ouyang, M., Li, X., Ma, J., Chi, W., Xiao, J., Zou, M., Chen, F., Lu, C., and Zhang, L. (2011). LTD is a protein required for sorting light-harvesting chlorophyll-binding proteins to the chloroplast SRP pathway. Nat. Commun. **2:** 277.

Paieri, F., Tadini, L., Manavski, N., Kleine, T., Ferrari, R., Morandini, P., Pesaresi, P., Meurer, J., and Leister, D. (2018). The DEAD-box RNA helicase RH50 is a 23S–4.5S rRNA maturation factor that functionally overlaps with the plastid signaling factor GUN1. Plant Physiol. **176:** 634–648.

Paukstelis, P.J., Chen, J.H., Chase, E., Lambowitz, A.M., and Golden, B.L. (2008). Structure of a tyrosyl-tRNA synthetase splicing factor bound to a group I intron RNA. Nature **451:** 94–97.

Peng, L., Ma, J., Chi, W., Guo, J., Zhu, S., Lu, Q., Lu, C., and Zhang, L. (2006). LOW PSII ACCUMULATION1 is involved in efficient assembly of photosystem II in Arabidopsis thaliana. Plant Cell **18:** 955–969.

Perez-Riverol, Y., et al. (2019). The PRIDE database and related tools and resources in 2019: Improving support for quantification data. Nucleic Acids Res. **47:** D442–D450.

Phadtare, S. (2011). Unwinding activity of cold shock proteins and RNA metabolism. RNA Biol. **8:** 394–397.

Phadtare, S., Inouye, M., and Severinov, K. (2002a). The nucleic acid melting activity of *Escherichia coli* CspE is critical for transcription antitermination and cold acclimation of cells. J. Biol. Chem. **277:** 7239–7245.

Phadtare, S., Tyagi, S., Inouye, M., and Severinov, K. (2002b). Three amino acids in *Escherichia coli* CspE surface-exposed aromatic patch are critical for nucleic acid melting activity leading to transcription antitermination and cold acclimation of cells. J. Biol. Chem. **277:** 46706–46711.

Powikrowska, M., Oetke, S., Jensen, P.E., and Krupinska, K. (2014). Dynamic composition, shaping and organization of plastid nucleoids. Front. Plant Sci. **5:** 424.

Prikryl, J., Rojas, M., Schuster, G., and Barkan, A. (2011). Mechanism of RNA stabilization and translational activation by a pentatricopeptide repeat protein. Proc. Natl. Acad. Sci. USA **108:** 415–420.

Régnier, P., Grunberg-Manago, M., and Portier, C. (1987). Nucleotide sequence of the pnp gene of *Escherichia coli* encoding polynucleotide phosphorylase. Homology of the primary structure

of the protein with the RNA-binding domain of ribosomal protein S1. J. Biol. Chem. **262:** 63–68.

Rojas, M., Ruwe, H., Miranda, R.G., Zoschke, R., Hase, N., Schmitz-Linneweber, C., and Barkan, A. (2018). Unexpected functional versatility of the pentatricopeptide repeat proteins PGR3, PPR5 and PPR10. Nucleic Acids Res. **46:** 10448–10459.

Rubio, V., Shen, Y., Saijo, Y., Liu, Y., Gusmaroli, G., Dinesh-Kumar, S.P., and Deng, X.W. (2005). An alternative tandem affinity purification strategy applied to Arabidopsis protein complex isolation. Plant J. **41:** 767–778.

Schmitz-Linneweber, C., Williams-Carrier, R., and Barkan, A. (2005). RNA immunoprecipitation and microarray analysis show a chloroplast Pentatricopeptide repeat protein to be associated with the 5′ region of mRNAs whose translation it activates. Plant Cell **17:** 2791–2804.

Schwarz, C., Elles, I., Kortmann, J., Piotrowski, M., and Nickelsen, J. (2007). Synthesis of the D2 protein of photosystem II in *Chlamydomonas* is controlled by a high molecular mass complex containing the RNA stabilization factor Nac2 and the translational activator RBP40. Plant Cell **19:** 3627–3639.

Shevchenko, A., Tomas, H., Havlis, J., Olsen, J.V., and Mann, M. (2006). In-gel digestion for mass spectrometric characterization of proteins and proteomes. Nat. Protoc. **1:** 2856–2860.

Stern, D.B., Goldschmidt-Clermont, M., and Hanson, M.R. (2010). Chloroplast RNA metabolism. Annu. Rev. Plant Biol. **61:** 125–155.

Stoppel, R., and Meurer, J. (2013). Complex RNA metabolism in the chloroplast: An update on the *psbB* operon. Planta **237:** 441–449.

Stoppel, R., Lezhneva, L., Schwenkert, S., Torabi, S., Felder, S., Meierhoff, K., Westhoff, P., and Meurer, J. (2011). Recruitment of a ribosomal release factor for light- and stress-dependent regulation of *petB* transcript stability in *Arabidopsis* chloroplasts. Plant Cell **23:** 2680–2695.

Stoppel, R., Manavski, N., Schein, A., Schuster, G., Teubner, M., Schmitz-Linneweber, C., and Meurer, J. (2012). RHON1 is a novel ribonucleic acid-binding protein that supports RNase E function in the *Arabidopsis* chloroplast. Nucleic Acids Res. **40:** 8593–8606.

Sun, T., Germain, A., Giloteaux, L., Hammani, K., Barkan, A., Hanson, M.R., and Bentolila, S. (2013). An RNA recognition motif-containing protein is required for plastid RNA editing in *Arabidopsis* and maize. Proc. Natl. Acad. Sci. USA **110:** E1169–E1178.

Takenaka, M., Zehrmann, A., Verbitskiy, D., Kugelmann, M., Härtel, B., and Brennicke, A. (2012). Multiple organellar RNA editing factor (MORF) family proteins are required for RNA editing in mitochondria and plastids of plants. Proc. Natl. Acad. Sci. USA **109:** 5104–5109.

Till, B., Schmitz-Linneweber, C., Williams-Carrier, R., and Barkan, A. (2001). CRS1 is a novel group II intron splicing factor that was derived from a domain of ancient origin. RNA **7:** 1227–1238.

Timmis, J.N., Ayliffe, M.A., Huang, C.Y., and Martin, W. (2004). Endosymbiotic gene transfer: Organelle genomes forge eukaryotic chromosomes. Nat. Rev. Genet. **5:** 123–135.

Walter, M., Chaban, C., Schütze, K., Batistic, O., Weckermann, K., Näke, C., Blazevic, D., Grefen, C., Schumacher, K., Oecking, C., Harter, K., and Kudla, J. (2004). Visualization of protein interactions in living plant cells using bimolecular fluorescence complementation. Plant J. **40:** 428–438.

Wang, F., Johnson, X., Cavaiuolo, M., Bohne, A.V., Nickelsen, J., and Vallon, O. (2015). Two *Chlamydomonas* OPR proteins stabilize chloroplast mRNAs encoding small subunits of photosystem II and cytochrome b_6 *f.* Plant J. **82:** 861–873.

Weber, M.H., and Marahiel, M.A. (2003). Bacterial cold shock responses. Sci. Prog. **86:** 9–75.

Weidmann, C.A., Qiu, C., Arvola, R.M., Lou, T.F., Killingsworth, J., Campbell, Z.T., Tanaka Hall, T.M., and Goldstrohm, A.C. (2016). Drosophila Nanos acts as a molecular clamp that modulates the RNA-binding and repression activities of Pumilio. eLife **5:** e17096.

Williams, P.M., and Barkan, A. (2003). A chloroplast-localized PPR protein required for plastid ribosome accumulation. Plant J. **36:** 675–686.

Williams-Carrier, R., Kroeger, T., and Barkan, A. (2008). Sequence-specific binding of a chloroplast pentatricopeptide repeat protein to its native group II intron ligand. RNA **14:** 1930–1941.

Xia, B., Ke, H., and Inouye, M. (2001). Acquirement of cold sensitivity by quadruple deletion of the cspA family and its suppression by PNPase S1 domain in *Escherichia coli.* Mol. Microbiol. **40:** 179–188.

Yang, C., Wang, L., Siva, V.S., Shi, X., Jiang, Q., Wang, J., Zhang, H., and Song, L. (2012). A novel cold-regulated cold shock domain containing protein from scallop *Chlamys farreri* with nucleic acid-binding activity. PLoS One **7:** e32012.

Yang, X.F., Wang, Y.T., Chen, S.T., Li, J.K., Shen, H.T., and Guo, F.Q. (2016). PBR1 selectively controls biogenesis of photosynthetic complexes by modulating translation of the large chloroplast gene *Ycf1* in *Arabidopsis.* Cell Discov. **2:** 16003.

Zerges, W. (2000). Translation in chloroplasts. Biochimie **82:** 583–601.

Zhang, L., Paakkarinen, V., van Wijk, K.J., and Aro, E.M. (1999). Co-translational assembly of the D1 protein into photosystem II. J. Biol. Chem. **274:** 16062–16067.

Zhelyazkova, P., Hammani, K., Rojas, M., Voelker, R., Vargas-Suárez, M., Börner, T., and Barkan, A. (2012). Protein-mediated protection as the predominant mechanism for defining processed mRNA termini in land plant chloroplasts. Nucleic Acids Res. **40:** 3092–3105.

Zhou, J., Li, F., Wang, J.L., Ma, Y., Chong, K., and Xu, Y.Y. (2009). Basic helix-loop-helix transcription factor from wild rice (OrbHLH2) improves tolerance to salt- and osmotic stress in Arabidopsis. J. Plant Physiol. **166:** 1296–1306.

Zoschke, R., and Bock, R. (2018). Chloroplast translation: Structural and functional organization, operational control, and regulation. Plant Cell **30:** 745–770.

Zoschke, R., Watkins, K.P., and Barkan, A. (2013). A rapid ribosome profiling method elucidates chloroplast ribosome behavior in *vivo.* Plant Cell **25:** 2265–2275.